

## *Hubble Space Telescope* OBSERVATIONS OF SHORT GRB HOST GALAXIES: MORPHOLOGIES, OFFSETS, AND LOCAL ENVIRONMENTS

W. FONG<sup>1</sup>, E. BERGER<sup>1</sup>, & D. B. FOX<sup>2</sup>

*Draft version August 13, 2024*

### ABSTRACT

We present the first comprehensive analysis of *Hubble Space Telescope* (*HST*) observations of short-duration gamma-ray burst (GRB) host galaxies. These observations allow us to characterize the galactic and local environments of short GRBs as a powerful constraint on the nature of their progenitors. Using the *HST* data for 10 short GRB hosts we determine the host morphological properties, measure precise physical and host-normalized offsets relative to the galaxy centers, and study the locations of short GRBs relative to their host light distributions. We find that most short GRB hosts have exponential disk profiles, characteristic of late-type galaxies, but with a median size that is twice as large as that of long GRB hosts, commensurate with their higher luminosities. The observed distribution of projected physical offsets, supplemented by ground-based measurements, has a median of  $\sim 5$  kpc, about 5 times larger than for long GRBs, and in good agreement with predicted offset distributions for NS-NS binary mergers. For the short GRB population as a whole we find the following robust constraints: (i)  $\sim 25\%$  have projected offsets of  $\leq 10$  kpc; and (ii)  $\sim 5\%$  have projected offsets of  $\leq 20$  kpc. We find no clear systematic trends for the offset distribution of short GRBs with and without extended soft emission. While the physical offsets are larger than for long GRBs, the distribution of host-normalized offsets is nearly identical due to the larger size of short GRB hosts. Finally, unlike long GRBs, which are concentrated in the brightest regions of their host galaxies, short GRBs appear to under-represent the light distribution of their hosts; this is true even in comparison to core-collapse and Type Ia supernovae. Based on these results, we conclude that short GRBs are consistent with a progenitor population of NS-NS binaries, but partial contribution from prompt or delayed magnetar formation is also consistent with the data. Our study underscores the importance of future *HST* observations of the larger *existing* and growing sample of short GRB hosts, which will allow us to delineate the properties of the progenitor population.

*Subject headings:* gamma-rays:bursts

### 1. INTRODUCTION

The galactic and local environments of cosmic explosions provide powerful insight into the nature of their progenitors. For example, past studies of supernova (SN) environments have demonstrated that Type Ia and Type Ib/Ic/II events arise from distinct progenitor systems since the former are located in all types of galaxies, while the latter occur only in star forming galaxies, pointing to a direct link with massive stars (e.g., van den Bergh et al. 2005). In a similar vein, long-duration gamma-ray bursts (GRBs; duration,  $T_{90} \geq 2$  s) have been linked with massive stars through their exclusive association with star forming galaxies (e.g., Bloom et al. 1998; Djorgovski et al. 1998; Fruchter et al. 1999). Short-duration GRBs, on the other hand, are now known to reside in all types of galaxies (Berger et al. 2005; Fox et al. 2005; Gehrels et al. 2005; Bloom et al. 2006; Berger 2009). Moreover, even the star forming host galaxies of short GRBs differ from those of long GRBs; they have higher luminosities and metallicities, and lower specific star formation rates (Berger 2009). The difference between long and short GRB host galaxies, along with the lack of SN associations for short GRBs (Berger et al. 2005; Fox et al. 2005; Gehrels et al. 2005; Hjorth et al. 2005; Bloom et al. 2006; Soderberg et al. 2006), demonstrate that they have distinct progenitor populations. In particular, at least some short GRBs are associated with an older progenitor population.

Equally important are the local, sub-galactic environments. In the case of long GRBs, the distribution of their projected physical and host-normalized offsets relative to the host centers matches the overall expected distribution for massive stars in an exponential disk (Bloom et al. 2002). An analysis of the brightness distribution at the locations of long GRBs indicates that they are disproportionately concentrated on the brightest regions of their hosts, primarily in comparison to core-collapse SNe, which follow the overall light distribution of their hosts (Fruchter et al. 2006). Both of these studies have relied on high angular resolution *Hubble Space Telescope* (*HST*) imaging observations. Preliminary studies of short GRB offsets (Berger et al. 2005; Fox et al. 2005; Bloom & Prochaska 2006; Soderberg et al. 2006; Troja et al. 2008; D’Avanzo et al. 2009) reveal somewhat larger projected physical offsets than for long GRBs, and have also led to a claimed trend of smaller offsets for short GRBs with extended X-ray emission (Troja et al. 2008). No study of the locations of short GRBs relative to their hosts light distribution has been published so far.

Progenitor models of short GRBs lead to distinct predictions about the distribution of host properties and the local environments of short GRBs (measured by their offsets and location relative to the host light distribution). In particular, the popular model of neutron star and/or black hole binary mergers (NS-NS/NS-BH; Eichler et al. 1989; Narayan et al. 1992) predicts larger offsets than for the massive star progenitors of long GRBs due to potential systemic velocity kicks. Various authors have employed population synthesis models to predict the distribution of offsets by convolving distributions of kick velocities, merger timescale, and galaxy masses (Bloom et al.

<sup>1</sup> Harvard-Smithsonian Center for Astrophysics, 60 Garden Street, Cambridge, MA 02138

<sup>2</sup> Department of Astronomy and Astrophysics, Pennsylvania State University, 525 Davey Laboratory, University Park, PA 16802

1999; Fryer et al. 1999; Belczynski et al. 2006). For Milky Way mass galaxies, appropriate for short GRB hosts (Berger 2009), the predicted offset distributions have a median of 5–10 kpc, with a broad tail extending to tens of kpc. On the other hand, progenitor models that invoke magnetars, either from a young population or through delayed formation in a WD-WD merger or white dwarf accretion-induced collapse (Levan et al. 2006b; Metzger et al. 2008), are expected to have a modest offset distribution since these systems do not experience kicks. Similarly, any systematic differences in the progenitors of short GRBs with and without extended X-ray emission may be revealed in the offset distribution and specific sub-galactic environments.

To confront these models with observations we require high angular resolution imaging, best provided by *HST*. Such observations provide detailed information on the host galaxy morphological properties (e.g., exponential disk versus de Vaucouleurs profile, effective radius), as well as the ability to precisely measure offsets and the distribution of short GRBs relative to their host light. *HST* observations have served as the backbone for detailed studies of long GRB environments and host galaxy morphologies (Bloom et al. 2002; Fruchter et al. 2006; Wainwright et al. 2007). To date, *HST* observations of only 3 short GRBs have been published (050709: Fox et al. 2005; 060121: Levan et al. 2006a; 080503: Perley et al. 2009), and in only one case (050709) was the host morphology addressed.

Here we present the first comprehensive analysis of all short GRB host galaxies observed with *HST* to date<sup>3</sup>. Using these observations we determine the host morphologies and structural properties (§3), we calculate precise physical and host-normalized offsets using accurate astrometry relative to ground-based afterglow images (§4), and we construct the first distribution of short GRB locations relative to their host light (§5). We draw conclusions in the context of progenitor models in §6. Throughout the paper we compare and contrast the results of our analysis with similar studies of long GRBs.

We find that: (i) the short GRB hosts have systematically larger effective radii than long GRB hosts, in good agreement with their higher luminosities; (ii) the observed short GRB projected physical offset distribution has a median of about 5 kpc, about a factor of 5 times larger than long GRBs, while for the population as a whole & 25% have projected offsets of > 10 kpc, and & 5% have projected offsets of > 20 kpc; (iii) both the observed physical offset distribution and the robust constraints closely match the predicted offset distribution of NS-NS binaries; and (iv) short GRBs uniformly trace the light distribution of their hosts, similar to core-collapse SNe, but distinct from long GRBs.

## 2. HUBBLE SPACE TELESCOPE DATA REDUCTION AND ANALYSIS

### 2.1. Sample

We present *HST* optical observations of ten short GRB host galaxies obtained with the Advanced Camera for Surveys (ACS) and the Wide-Field Planetary Camera 2 (WFPC2). The data were obtained as part of programs 10119, 10624, and 10917 (PI: Fox), as well as 10780 and 11176 (PI: Fruchter). These programs targeted all short GRBs with optical and X-ray (XRT) positions from May 2005 to December 2006,

<sup>3</sup> We do not repeat the analysis for GRB 080503 since no convincing host galaxy was identified (Perley et al. 2009). Future *HST* ACS or WFPC3 observations will provide better constraints on an underlying host than available from the existing WFPC2 observations.

which were visible during *HST* 2-gyro operations. In this time frame, the only short burst that was not observed was GRB 060801. Thus, the sample in this paper is nearly complete in relation to the short GRBs with optical/X-ray afterglows<sup>4</sup>. The *HST* observations of GRBs 050709 and 060121 have been published previously by Fox et al. (2005) and Levan et al. (2006a), respectively, but we re-analyze them here in a uniform fashion and perform a more comprehensive analysis of the host morphology and burst environment. Seven of the nine bursts have been localized to sub-arcsecond precision from optical afterglow detections, and five have known redshifts (Table 1); we use a constraint of  $z < 1.4$  for GRB 051210 (Berger et al. 2007).

Six of the seven short GRBs with sub-arcsecond localization are robustly associated with host galaxies<sup>5</sup> (we present a host identification for GRB 060313 in this paper; see Appendix A). The sole exception is GRB 061201, for which we explore two possible host galaxy associations based on the *HST* observations (see Appendix B); previously only one galaxy (at  $z = 0.11$ ) was considered a potential host (Berger et al. 2007; Stratta et al. 2007). Details of the GRB properties and the *HST* observations are provided in Table 1.

Throughout the paper we use the standard cosmological parameters,  $H_0 = 71 \text{ km s}^{-1} \text{ Mpc}^{-1}$ ,  $\Omega_m = 0.27$ , and  $\Omega_\Lambda = 0.73$ . All reported magnitudes are corrected for Galactic extinction using Schlegel et al. (1998) dust maps.

### 2.2. Hubble Space Telescope Data Reduction

We retrieved pre-processed images from the *HST* archive<sup>6</sup> for all available short GRBs. We distortion-corrected and combined the individual exposures using the IRAF task `multidrizzle` (Fruchter & Hook 2002; Koekemoer et al. 2002). For the ACS images we used `pixfrac=0.8` and `pixscale=0.05 arcsec pixel-1`, while for the WFPC2 images, we used `pixfrac=1.0` and `pixscale=0.0498 arcsec pixel-1`, half of the native pixel scale. The final drizzled images, flux-calibrated to the AB magnitude system according to the ACS and WFPC2 zeropoints, are shown in Figures 1-10.

### 2.3. Surface Brightness Profile Fitting

We use two methods to fit the surface brightness profiles of the short GRB host galaxies. First, we use the `galfit` software package (Peng et al. 2007) to construct the best two-dimensional ellipsoidal model of each galaxy image. Second, we use the IRAF task `ellipse` to produce elliptical intensity isophotes and to construct one-dimensional radial surface brightness profiles. We further use `ellipse` to measure the integrated AB magnitude for each galaxy (listed in Table 1).

#### 2.3.1. galfit

As an input to `galfit` we generate point-spread-function (PSF) models for each instrument and filter combination using the `tinytim` software package. We assume a constant spectrum in  $F_\lambda$ ; the difference in the 90% encircled energy

<sup>4</sup> We do not include in this analysis GRBs 051227, 060505, and 060614 all of which had durations well beyond 2 s, even when isolating the initial “short” emission episode. The *HST* data for GRBs 060505 and 060614 were published in Ofek et al. (2007) and Gal-Yam et al. (2007), respectively.

<sup>5</sup> For a complete discussion of the galaxy associations we refer the reader to the following papers: GRB 050709: Fox et al. (2005); GRB 050724: Berger et al. (2005); GRB 051221: Soderberg et al. (2006); GRB 060121: Levan et al. (2006a); GRB 061006: Berger et al. (2007) and D’Avanzo et al. (2009).

<sup>6</sup> see <http://archive.stsci.edu/hst/>.

width of the PSF for a spectral index ranging from  $-2$  to  $0$  is only 1%. We additionally correct for distortion in the ACS instrument, and use a sub-sampling factor of 2 for WFPC2 to appropriately account for the reduced pixel scale in the drizzled images.

In each observation we fit the host galaxy image with a PSF-convolved Sérsic profile:

$$I(r) = I_e \exp[-n(r/r_e)^{1/n} - 1]g; \quad (1)$$

where  $n$  is the concentration parameter ( $n = 1$  is equivalent to an exponential disk profile, while  $n = 4$  is the de Vaucouleurs profile),  $I_e = 2n - 1 = 3 + 4 = 405n + 46 = 25515n^2$  is a constant that is coupled to the value of  $n$  (Ciotti & Bertin 1999),  $r_e$  is the effective radius, and  $I_e$  is the effective surface brightness in flux units. In the subsequent discussion, tables, and figures we use surface brightness in units of  $\text{mag arcsec}^{-2}$ , designated as  $I_e$ .

In all cases we fit the host galaxies with a single<sup>7</sup> Sérsic profile and allow the parameters to vary freely. The resulting best-fit values of  $n$ ,  $r_e$ , and  $I_e$ , as well as the integrated AB magnitudes are provided in Table 2. For host galaxies that are detected at a low signal-to-noise ratio we find that a wide range of  $n$  values can account for the observed morphology. In these cases we fit the host galaxies with  $n$  fixed at values of 1 and 4, and provide the results of both models in Table 2.

The `galfit` models and residual images for all instrument/filter combinations are shown in Figures 1-9. Objects for which both  $n = 1$  and  $n = 4$  models provide an adequate fit are shown for both cases.

### 2.3.2. Radial Profiles from IRAF/ellipse

We use `ellipse` to generate elliptical isophotes for each host galaxy, with the center and ellipticity of each isophote allowed to vary<sup>8</sup>. The resulting radial surface brightness profiles in units of  $\text{AB mag arcsec}^{-2}$  are shown in Figure 11. We fit each profile with a Sérsic model (Equation 1) using  $n$ ,  $r_e$ , and  $I_e$  as free parameters. The best-fit values are listed in Table 2, and the resulting models are shown in Figure 11. We find adequate fits in all cases, although some host galaxies clearly exhibit radial complexity due to irregular structure and/or an edge-on orientation.

### 2.4. Astrometry

To determine the location of each short GRB relative to its host galaxy we perform differential astrometry using optical and near-IR images of the afterglows<sup>9</sup>. With the exception of GRB 050709, whose afterglow is directly detected in *HST*/ACS observations, we use ground-based images from Magellan, Gemini, and the VLT. The astrometric tie between the afterglow and host images is performed using point sources in common between the two images; the source of the afterglow image and the number of astrometric tie objects are listed in Table 3. In the case of ground-based to *HST* astrometry we use a range of 15–85 common objects, with the number depending on the density of stellar sources in the field, the depth of the images, and the field-of-view. To determine the

astrometric tie we use the IRAF astrometry routine `ccmap`. We find that a second-order polynomial, with six free parameters corresponding to a shift, scale, and rotation in each coordinate, provides a robust astrometric tie in all cases. The resulting rms values are  $\sigma_{\text{GB! HST}} = 13 - 30$  mas (Table 3).

We next consider the uncertainty in the afterglow position from each ground-based image. The centroiding accuracy depends on the size of the PSF and the signal-to-noise ratio (S/N) of the afterglow detection,  $\sigma_{\text{centroid}} = \text{FWHM} / (S/N)$ . We determine  $\sigma_{\text{GRB}}$  for each GRB using the `SExtractor` program<sup>10</sup> (Table 3). In the case of GRBs 050724 and 051221 we find that  $\sigma_{\text{GRB}}$  is significantly smaller than  $\sigma_{\text{GB! HST}}$ ; for GRBs 060121, 060313, and 061006 the two sources of uncertainty are comparable; and for GRB 061201  $\sigma_{\text{GRB}}$  dominates. The afterglows of GRBs 050509b, 051210, and 060502b have only been detected in X-rays, with the *Swift* X-ray Telescope (XRT), and as a result their positional uncertainty is  $\sigma_{\text{GRB}} = 1.7 - 5.8''$  (Table 3). We note that the XRT positions from the catalogs of Butler (2007) and Evans et al. (2009) exhibit relative offsets of  $5.6''$  (GRB 050509b),  $3.0''$  (GRB 051210), and  $2.9''$  (GRB 060502b) suggesting that the true positional uncertainties (including systematics) are larger than their quoted statistical uncertainties.

The final source of uncertainty in the relative position of the GRB and host galaxy is the centroiding accuracy of the host in the *HST* images. To determine this uncertainty we again use `SExtractor`. The resulting values of  $\sigma_{\text{gal}}$  are listed in Table 3. We find that for GRBs 050724, 051221, and 061006 the host centroid uncertainty is smaller than both  $\sigma_{\text{GB! HST}}$  and  $\sigma_{\text{GRB}}$ , while for GRBs 060121 and 060313  $\sigma_{\text{gal}}$  is comparable to  $\sigma_{\text{GRB}}$ . The combined offset uncertainties are listed in Table 3.

A much more accurate relative position is available for GRB 050709 since the afterglow was detected in *HST*/ACS images (Fox et al. 2005). The limiting factor is thus  $\sigma_{\text{gal}}$  for the afterglow and host. We find from the first *HST*/ACS observation (2005 July 15.6 UT) that  $\sigma_{\text{GRB}} = 1$  mas, while  $\sigma_{\text{gal}} = 1.4$  mas. In addition, we also astrometrically tie the final epoch of ACS imaging and the WFPC2 image to the first epoch. Since the afterglow is no longer detected in these images, this allows us to study the burst environment. For the final ACS image we find  $\sigma_{\text{HST! HST}} = 8$  mas, while for the WFPC2 image we find  $\sigma_{\text{HST! HST}} = 14.5$  mas. These uncertainties clearly dominate over the centroiding errors of the afterglow and host galaxy. We do note, however, that the complex morphology of the host galaxy (§3) introduces a systematic uncertainty in the definition of the host “center”. By varying the signal-to-noise threshold in `SExtractor`, we find that the centroid of the host shifts by as much as 50 mas, which dominates over the statistical uncertainty in the source position.

Similarly, we find a more accurate offset for GRB 050724 from a detection of the afterglow and host in ground-based near-IR images (Berger et al. 2005). The combined afterglow and host centroid uncertainty in these images is about 6 mas, compared to a total uncertainty of 20–25 mas for the *HST* images.

### 2.5. Host Light Distribution

To determine the brightness of the GRB location relative to the host light distribution, we follow the methodology of Fruchter et al. (2006) and Kelly et al. (2008) and calculate

<sup>7</sup> In the case of GRBs 050509b, 050709, 060121, and 061006 we fit additional Sérsic and point-source components to account for foreground/background objects. These components are not considered to be part of the host galaxy.

<sup>8</sup> For the hosts of GRBs 060121 and 060313, with low signal-to-noise detections, the center and ellipticity were held fixed throughout the fit.

<sup>9</sup> Optical afterglows have not been detected in the case of GRBs 050509b and 051210.

<sup>10</sup> <http://sextractor.sourceforge.net/>

from each galaxy image the fraction of total light in pixels fainter than the afterglow position. Six bursts have differential astrometric positions of better than 1 pixel (050709, 050724, 051221a, 060121, 060313 and 061006; Table 3). For each image we create an intensity histogram of a  $5'' \times 5''$  region centered on the host galaxy and determine a 1 $\sigma$  cut-off level for the host by fitting a Gaussian profile to the sky brightness distribution (equivalent to a signal-to-noise ratio cut-off of 1). We then plot the pixel flux distribution above the appropriate cut-off level for a region surrounding the host, and determine the fraction of light in pixels fainter than the afterglow pixel; see Table 4.

### 3. MORPHOLOGICAL ANALYSIS

Using the results of the `galfit` analysis and the radial surface brightness profiles we first classify the short GRB hosts in terms of their Sérsic  $n$  values. From the `galfit` analysis we find that three hosts (GRBs 050709, 051221a, and 061006) are best modeled with  $n = 1$ , corresponding to an exponential disk profile, while two hosts (GRBs 050509b and 050724) are best modeled with  $n = 3$  and  $n = 5.6$ , respectively, typical of elliptical galaxies. We note that GRB 050724 possibly exhibits weak spiral structure, which may explain the resulting value of  $n = 3$  (see Figure 3 and Malesani et al. 2007), but this putative spiral structure is clearly sub-dominant relative to the elliptical structure. The final three hosts (GRBs 051210, 060121, and 060313) are equally well modeled in `galfit` with a wide range of  $n$  values, and we provide results for both  $n = 1$  and  $n = 4$  in Table 2.

We find identical results using Sérsic model fits to the one-dimensional radial surface brightness profiles generated with `ellipse` (Figure 11 and Table 2). However, with this approach we find best-fit values of  $n = 1$  for the three host galaxies with ambiguous `galfit` results, suggesting that they are indeed better modeled as exponential disks. We therefore conclude that of the eight short GRB host galaxies studied here only two can be robustly classified as elliptical galaxies based on their morphology. A similar fraction was determined independently from spectroscopic observations (Berger 2009). The distribution of  $n$  values is shown in Figure 12.

As can be seen from the `galfit` results, the Sérsic models of the two elliptical hosts exhibit significant residuals (Figures 1 and 3). This is a well-known effect for bright elliptical galaxies, which generally require a multi-parameter power-law plus Sérsic fit that accounts for a flatter core than expected in the de Vaucouleurs model (Trujillo et al. 2004). Since we are here mainly interested in the distribution of  $n$  values and a comparison to long GRB hosts, we retain the simple Sérsic formulation.

We also find significant residuals for a one-component Sérsic fit of the host galaxy of GRB 050709, which has an irregular morphology dominated by an exponential profile (Figure 2). This is the only clearly irregular galaxy in the sample. Finally, we find that the hosts of GRBs 051210, 060121, and 061006 exhibit significant bulges, clearly seen in their radial surface brightness profiles (Figure 11). For the host of GRB 061006, which was observed in two filters, the bulge component is more significant in the F814W filter than in the F555W filter, as expected for an older stellar population; the burst appears to coincide with this bulge component (Figure 9).

The `galfit` and radial profile fits also yield values of the effective radius,  $r_e$ , for each host galaxy. We find a range

of  $0.2 - 5.8''$ , corresponding to physical scales<sup>11</sup> of about  $1.4 - 21$  kpc. The smallest effective radius is measured for the host of GRB 060313, while the host of GRB 050509b has the largest effective radius. The median value is  $r_e = 3.5$  kpc. We adopt the best-fit values from the radial surface brightness profiles, and plot the resulting distribution, as well as  $r_e$  as a function of  $n$ , in Figure 12.

Finally, the effective surface brightness values range from  $21$  to  $27$  AB mag arcsec<sup>-2</sup>. The galaxy with the highest surface brightness is the host of GRB 050724, while the lowest surface brightness is measured for the host of GRB 060121. The integrated magnitudes range from about 16.3 AB mag (GRB 050509b) to 26.4 AB mag (GRB 060313).

#### 3.1. Comparison to Long GRB Host Galaxies

A comprehensive morphological analysis of long GRB host galaxies using *HST* observations with the STIS, WFPC2, and ACS instruments has been carried out by Conselice et al. (2005) and Wainwright et al. (2007). In Figure 12 we compare the values of  $n$  and  $r_e$  measured for long GRB hosts by Wainwright et al. (2007) to the values measured here for short GRB hosts. Two clear trends emerge from this comparison. First, all long GRB hosts have  $n > 2.5$ , and the median value for the population is  $n = 1.1$  (Wainwright et al. 2007). Thus, all long GRB hosts are morphologically classified as exponential disks, while 2 of the 8 short GRB hosts studied here exhibit de Vaucouleurs profiles. However, for the hosts with  $n > 2$ , the distributions of  $n$  values for both populations appear to be similar.

Second, short GRB hosts have larger effective radii, with  $r_{e,i} = 3.5$  kpc, compared to  $r_{e,i} = 1.7$  kpc for long GRB hosts (Wainwright et al. 2007). A Kolmogorov-Smirnov (K-S) test indicates that the probability that the short and long GRB hosts are drawn from the same underlying distribution of host galaxy effective radii is only 0.04. If we remove from the sample GRBs 050509b and 051210 (which have only XRT positions) we find that the K-S probability is still only 0.09. Thus, we conclude with high significance that short GRB host galaxies are systematically larger than long GRB hosts, and that this result is not affected by host associations based on XRT positions. The larger sizes of short GRB hosts are expected in the context of the galaxy size-luminosity relation (e.g., Freeman 1970). We recently showed that short GRB hosts are systematically more luminous than long GRB hosts by about  $M_B = 1.2$  mag (Berger 2009) and therefore their sizes are expected to be correspondingly larger.

An additional striking difference between the hosts of long and short GRBs is the apparent dearth of interacting or irregular galaxies in the short GRB sample. Of the eight host galaxies studied here, we find only one irregular galaxy (GRB 050709) and none that appear to be undergoing mergers. In contrast, the fraction of long GRB hosts with an irregular or merger/interaction morphology is about 30–60% (Wainwright et al. 2007). The interpretation for this high merger/interaction fraction in the long GRB sample is that such galaxies are likely undergoing intense star formation activity triggered by the merger/interaction process, and are therefore suitable sites for the production of massive stars.

<sup>11</sup> For the faint hosts without a known redshift (GRBs 051210, 060121, 060313, and possibly 061201) we assume  $z = 1$  (Berger et al. 2007), and take advantage of the relative flatness of the angular diameter distance as a function of redshift beyond  $z = 0.5$ .

The lack of morphological merger signatures in the short GRB sample indicates that if any of the hosts have undergone significant mergers in the past, the delay time between the merger and the production of a short GRB is  $\lesssim 10^9$  yr (e.g., Barnes & Hernquist 1992).

#### 4. OFFSETS

We next turn to an analysis of short GRB offsets relative to the centers of their host galaxies. Based on the astrometric tie of the *HST* host observations to ground-based afterglow observations, we find that the projected offsets are in the range of

$0.12 - 17.7^{+0.0}$  (Table 3). The corresponding projected physical offsets are about 1–64 kpc, with a median value of about 3 kpc. The largest offsets are measured for GRBs 050509b and 051210, but these are based on *Swift*/XRT positions with statistical uncertainties of about 12 and 18 kpc, respectively (and possibly larger if we consider systematic uncertainties; §2.4). If we consider only the bursts with sub-arcsecond afterglow positions we find that the largest offset is 3.7 kpc (GRB 050709), and that the median offset for the 6 bursts is 2.2 kpc. In the case of GRB 061201 the host association remains ambiguous (see Appendix B), but even for the nearest detected galaxy the offset is about 14.2 kpc. The obvious caveat is that an undetected fainter host, with  $\lesssim 25.5$  AB mag, may be located closer to the GRB position.

To investigate the offset distribution in greater detail we supplement the values measured here with offsets for GRBs 070724, 071227, and 090510 from ground-based observations (Berger et al. 2009; Rau et al. 2009). In the case of GRBs 070724 and 071227 the optical afterglows coincide with the disks of apparent edge-on spiral galaxies (Berger et al. 2009; D’Avanzo et al. 2009). The offsets of the three bursts are 4.8, 14.8, and 5.5 kpc, respectively (Berger et al. 2009; Rau et al. 2009). For GRB 071227 we calculate the relative offset from our Magellan/IMACS observations and find a total ( $\delta_{\text{GRB}} + \delta_{\text{gal}}$ ) uncertainty of 65 mas, corresponding to 0.34 kpc at the redshift of the host<sup>12</sup>.

There are 7 additional events with optical afterglow identifications. Of these bursts, two (070707 and 070714b) coincide with galaxies (Piranomonte et al. 2008; Graham et al. 2009), but their offsets have not been measured by the respective authors. Based on the claimed coincidence we conservatively estimate an offset of  $\lesssim 0.5^{+0.0}$ , corresponding<sup>13</sup> to  $\lesssim 4$  kpc. Two additional bursts (070809 and 080503) do not have coincident host galaxies to deep limits, but the nearest galaxies are located about 6.5 and 20 kpc from the afterglow positions, respectively<sup>14</sup> (Perley et al. 2008, 2009). For the final three bursts (080905, 090305, and 090426) no deep host galaxy searches exist in the literature.

In addition to the bursts with sub-arcsecond positions, several hosts have been identified within XRT error circles in follow-up observations (GRBs 060801, 061210, 061217, 070429b, 070729, and 080123; Berger et al. 2007; Berger 2009), but in all of these cases the offsets are consistent

<sup>12</sup> This is significantly more precise than the large uncertainty of  $0.4^{+0.0}$  quoted by D’Avanzo et al. (2009) based on *absolute* astrometry; for offset measurements differential astrometry provides a better approach.

<sup>13</sup> GRB 070714b is located at  $z = 0.923$ , while the redshift of GRB 070707 is not known. Based on the faintness of the host,  $R = 27.3$  mag, we assume  $z = 1$  to calculate the physical offset.

<sup>14</sup> GRB 070809 is located 19.6 kpc from a galaxy at  $z = 0.219$ , and about  $2.3^{+0.0}$  from a much fainter galaxy, which at  $z \approx 1$  corresponds to 18.4 kpc. No host is detected at the position of GRB 080503 in deep *HST* observations, but a faint galaxy is located about  $0.8^{+0.0}$  away, which at  $z \approx 1$  corresponds to 6.5 kpc.

with zero, or may be as large as  $\sim 30$  kpc (e.g., Berger et al. 2007). For example, the offsets for GRBs 060801, 061210, and 070429b are  $19 \pm 16$  kpc,  $11 \pm 10$  kpc, and  $40 \pm 48$  kpc. We use 30 kpc as a typical upper limit on the offset for these 6 events. We note that no follow-up observations are available in the literature for most short GRBs with X-ray positions from 2008–2009. Finally, about  $1/4 - 1/3$  of all short GRBs discovered to date have only been detected in  $\gamma$ -rays, precluding a unique host galaxy association and an offset measurement.

The cumulative distribution of projected physical offsets for the GRBs with *HST* observations from this work, supplemented by the bursts with offsets or limits based on optical afterglow positions (070707, 070714b, 070724, 070809, 071227, 080503, and 090510) is shown in Figure 13. Also shown is the differential probability distribution,  $P(r)dr$ , taking into account the non-Gaussian errors on the radial offsets (see discussion in Appendix B of Bloom et al. 2002). We find that the median for this sample is about 5 kpc.

As evident from the discussion above, this is not a complete offset distribution; roughly an equal number of short GRBs have only limits or undetermined offsets due to their detection in just the X-rays or  $\gamma$ -rays<sup>15</sup>. Taking these events into account, our most robust inferences about the offset distribution of short GRBs are as follows:

At least 25% of all short GRBs have projected physical offsets of  $\lesssim 10$  kpc.

At least 5% of all short GRBs have projected physical offsets of  $\lesssim 20$  kpc.

At least 50% of all short GRBs have projected physical offsets of  $\lesssim 30$  kpc; this value includes the upper limits for the hosts identified within XRT error circles.

These robust constraints are shown in Figure 13.

Using the observed distribution and the robust constraints outlined above, we now provide a comparison with predicted distributions for NS-NS binaries in Milky Way type galaxies (Bloom et al. 1999; Fryer et al. 1999; Belczynski et al. 2006), appropriate for the observed luminosities of short GRB host galaxies (Berger 2009). We find good agreement between the observed distribution and those predicted by Bloom et al. (1999) and Belczynski et al. (2006). The offset distribution of Fryer et al. (1999), with a median of about 7 kpc, predicts larger offsets and therefore provides a poorer fit to the observed distribution, which has a median of about 5 kpc. However, all three predicted distributions accommodate the offset constraints. In particular, they predict about 60–75% of the offsets to be  $\lesssim 10$  kpc, about 80–90% to be  $\lesssim 30$  kpc, and about 10–25% of the offsets to be  $\lesssim 20$  kpc. Thus, the projected physical offsets of short GRBs are consistent with population synthesis predictions for NS-NS binaries. However, the observations are also consistent with partial contribution from other progenitor systems with no expected progenitor kicks, such as WD-WD binaries.

#### 4.1. Host-Normalized Offsets

To compare the offsets in a more uniform manner, we normalize the measured values by  $r_e$  for each host galaxy. We

<sup>15</sup> We do not consider the bursts that lack host searches since there is no a priori reason that these events (mainly from 2008–2009) should have a different offset distribution compared to the existing sample from 2005–2007.

use the  $r_e$  values measured from the one-dimensional radial surface brightness profiles from `ellipse` (see Figure 14 and Table 3) and find values ranging from about  $0.2 r_e$  for GRB 060121 to  $6.7 - 2.7 r_e$  for the Evans et al. (2009) XRT position of GRB 051210. The Butler (2007) position for GRB 051210, however, leads to an offset of  $4.65 - 4.60 r_e$ , consistent with a negligible offset. For the subset of 6 bursts with optical afterglow positions and secure host associations, 4 are located within  $1 r_e$ , while the remaining 2 bursts are located at about  $2 r_e$  (Figure 14). GRB 050509b, which has the largest physical offset, has a normalized offset of  $2 - 3 r_e$ , depending on which XRT position is used. Thus, with the exception of the ambiguous case of GRB 061201, we find that all of the available offsets are consistent with  $\leq 2 r_e$ . The large additional sample of physical offsets that we used above cannot be easily translated to host-normalized offsets at the present since none of the hosts have been observed with *HST*, thereby precluding a robust morphological analysis. This provides an impetus for future *HST* observations.

The differential probability distribution of host-normalized offsets for our *HST* sample, taking into account the non-Gaussian errors, is shown in Figure 15. We find that the median value for all 8 bursts is  $1 r_e$ . Moreover,  $\sim 20\%$  of the probability distribution is at large offsets of  $\geq 2.5 r_e$ .

#### 4.2. Comparison to Long GRB Host Galaxies

We compare our observed short GRB offsets with those of long GRBs from the sample of Bloom et al. (2002) in Figures 13-15. The offset distribution of long GRBs has been used to argue for a massive star progenitor population, and against NS-NS binaries (Bloom et al. 2002). The offset distribution for short GRBs is clearly shifted to larger physical scales. In particular, the median offset for the long GRBs is 1.1 kpc, about a factor of 5 times smaller than the median value for short GRBs. Similarly, no long GRB offsets are larger than about 7 kpc, whereas at least some short GRBs appear to have offsets in excess of 15 kpc.

However, the distinction between the two offset distributions is significantly reduced when we take into account the systematically larger sizes of short GRB host galaxies (Figure 12). The median normalized offset for long GRBs is about  $0.8 r_e$ , compared to about  $1 r_e$  for short GRBs. Similarly,  $20\%$  of the long GRB cumulative distribution has offsets of  $\geq 2.5 r_e$ , identical to the statistics for the short GRB offsets. Indeed, as can be seen from Figure 15, the cumulative host-normalized offset distributions for long GRBs and short GRBs with *HST* observations are nearly identical.

In the context of NS-NS binary progenitors, the close similarity in the normalized offset distributions can be interpreted to mean that most systems likely remain bound to their hosts (rather than ejected into the intergalactic medium), and/or have a relatively short delay time. These conclusions are tentative due to the small number of events with host-normalized offsets, but they can be further tested with future *HST* observations.

### 5. LIGHT DISTRIBUTION ANALYSIS

In addition to the offset analysis in the previous section, we study the local environments of short GRBs using a comparison of their local brightness to the host light distribution. This approach is advantageous because it is independent of galaxy morphology, and does not suffer from ambiguity in the definition of the host center (see Fruchter et al. 2006). We note that for the overall regular morphology of short GRB hosts

the definition of the host center is generally robust, unlike in the case of long GRBs (Fruchter et al. 2006; Wainwright et al. 2007). On the other hand, this approach has the downside that it requires precise pixel-scale positional accuracy. In our sample, this is the case for only 6 short bursts.

The fraction of host light in pixels fainter than the afterglow pixel brightness for each host/filter combination is summarized in Table 4. The cumulative light distribution histogram is shown in Figure 16. The shaded histogram represents the range defined by the dual filters for 5 of the 6 bursts. We find that the upper bound of the distribution is defined by the blue filters, indicating that short GRBs trace the rest-frame optical light of their hosts better than the rest-frame ultraviolet. This indicates that short GRB progenitors are likely to be associated with a relatively old stellar population, rather than a young and UV bright population.

The overall distribution has a median value of  $0.1 - 0.4$  (red); namely, only in about one-quarter of the cases,  $50\%$  of the host light is in pixels fainter than at the GRB location. Thus, the overall distribution of short GRB locations under-represents the host galaxies' light distribution. This is also true in comparison to the distribution for core-collapse SNe, which appear to track their host light (Fruchter et al. 2006), and even Type Ia SNe, which have a median of about 0.4 (Kelly et al. 2008). Thus, the progenitors of short GRBs appear to be more diffusely distributed than Type Ia SN progenitors.

#### 5.1. Comparison to Long GRB Host Galaxies

An extensive analysis of the brightness distribution at the location of long GRBs has been carried out by Fruchter et al. (2006). These authors find that long GRBs are more concentrated on the brightest regions of their hosts than expected from the light distribution of each host. In particular, they conclude that the probability distribution of GRB positions is roughly proportional to the surface brightness squared. As can be seen from Figure 16, short GRBs have a significantly more diffuse distribution relative to the host light than long GRBs. In particular, for the latter, the median light fraction is about 0.85 compared to about  $0.25 - 0.15$  for the short GRBs.

## 6. DISCUSSION AND IMPLICATIONS

Our extensive analysis of short GRB host galaxy morphologies and the burst local environments has important implications for the progenitor population. We address in particular the popular NS-NS merger model, as well as delayed magnetar formation via WD-WD mergers or WD accretion-induced collapse (Metzger et al. 2008).

### 6.1. Morphology

From the morphological analysis we find continued evidence that the bulk of short GRB host galaxies ( $\sim 3-4$ ) are late-type galaxies, in agreement with results from spectroscopic observations (Berger 2009). Moreover, as demonstrated by the systematic differences in luminosity, star formation rates, and metallicities between the star forming hosts of long and short GRBs (Berger 2009), we find here that short GRB hosts are systematically larger than long GRB hosts. These results indicate that the progenitors of the two GRB classes select different environments. The higher luminosities, larger sizes, and lower specific star formation rates of short GRB hosts suggest that their rate of occurrence is tied to galactic mass rather than to star formation activity. This result is in broad agreement with old progenitor populations

such as NS-NS, NS-BH, or WD-WD binaries, but it indicates that the bulk of short GRB progenitors are not young magnetars. This conclusion is also supported by the dearth of merger signatures, which point to delays of  $\sim 10^9$  yr relative to any merger-triggered star formation episodes.

### 6.2. Offsets

The differential offsets measured here from the *HST* observations provide the most precise values to date for short GRBs, with a total uncertainty of only  $\sim 10$ – $60$  mas, corresponding to  $\sim 30$ – $500$  pc. We find that none of the offsets are smaller than  $\sim 1$  kpc, while this is the median offset for long GRBs. On the other hand, a substantial fraction of the *measured* offsets are only a few kpc. The median offset for the *HST* observations supplemented by ground-based data is about 5 kpc (Figure 13), about 5 times larger than for long GRBs.

As discussed in detail in §4, the observed offset distribution is incomplete. About  $1/4$ – $1/3$  of all short GRBs have only  $\gamma$ -ray positions ( $\sim 1$ – $3^\circ$ ), and a similar fraction have only XRT positions, which generally lead to a range of offsets of  $\sim 0$ – $30$  kpc. Taking these limitations into account we find that the most robust constraints on the offset distribution are that  $\sim 25\%$  of all short GRBs have offsets of  $\sim 10$  kpc, and that  $\sim 5\%$  have offsets of  $\sim 20$  kpc. Both the observed offset distribution and these constraints are in good agreement with predictions for the offset distribution of NS-NS binaries in Milky Way type galaxies (Bloom et al. 1999; Fryer et al. 1999; Belczynski et al. 2006). However, at the present they cannot rule out at least a partial contribution from other progenitor systems such as delayed magnetar formation and even young magnetar flare. The apparent existence of large offsets in the sample suggests that these latter models are not likely to account for *all* short GRBs.

In contrast to the larger physical offsets of short GRBs, we find that the distribution of offsets normalized to the host galaxy effective radii exhibits much better agreement between long and short GRBs (Figure 15). The medians of the two distributions are similar ( $1$  versus  $0.8 r_e$  for short and long GRBs, respectively), and both populations have  $\sim 20\%$  probability for offsets of  $\sim 2.5 r_e$ . Naturally, due to the lack of *HST* observations for short GRBs from 2007–2009, the sample for which this analysis is possible is smaller than the sample with physical offsets. Thus, further *HST* observations of existing and future short GRB hosts are essential in order to determine whether the broad similarity in host-normalized offsets is robust. We stress that in the context of comparing short GRBs with various progenitor populations and with long GRBs, host-normalized offsets are the more relevant quantity. For example, the host-normalized distributions for massive stars in small and large galaxies will be similar even though their physical offsets will differ. We stress that population synthesis modelers should include an appropriate distribution of host galaxy sizes, and thereby provide predictions for host-normalized offsets.

In the context of implications for the progenitor population, a recent study of short GRB physical offsets by Troja et al. (2008) led these authors to claim that short GRBs with extended X-ray emission have systematically smaller offsets, possibly due to a systematic difference in the progenitors. Our *HST* sample includes three short GRBs with strong extended emission (050709, 050724, and 061006), and one GRB (060121) with possible extended emission (4.5  $\sigma$  significance; Donaghy et al. 2006). The physical offsets of these bursts are

about 3.7, 2.7, 1.3, and 1 kpc, respectively, leading to a mean offset of about 2.2 kpc. The physical offsets of the bursts without extended emission, but with precise afterglow positions (051221, 060313, and 061201) are 2.0, 2.3, and 14.2 or 32.5 kpc, respectively. The two events with no extended emission and with XRT positions (050509b and 051210) have offsets of about  $54 \pm 12$  and  $28 \pm 23$  kpc, respectively. If we include the ground-based sample with optical afterglow positions (see §4), we find that the bursts with apparent extended emission (070714b, 071227, 080513, and 090510; Barbier et al. 2007; Sakamoto et al. 2007; Ukwatta et al. 2009; Perley et al. 2009) have offsets of  $\sim 4$ , 14.8,  $\sim 20$ , and  $\sim 5.5$  kpc, while the bursts without extended emission (070724 and 070809) have offsets of 4.8 and  $\sim 6.5$  kpc. Thus, based on the sample of events with sub-arcsecond positions we find that  $6/8$  bursts with extended emission have offsets of  $\sim 5$  kpc and  $2/8$  have likely offsets of  $\sim 15$ – $20$  kpc. In the sample without extended emission we find that  $4/5$  have offsets of  $\sim 6$  kpc and  $1/5$  has a likely offset of  $\sim 14$ – $32$  kpc. Thus, we conclude that there is no significant difference in the two offset distributions.

The inclusion of events with only XRT positions does not change this conclusion. In particular, of the subset with no extended emission only GRB 050509b is likely to have a significant offset, while GRBs 051210, 060801, and 070429b have offsets ( $28 \pm 23$ ,  $19 \pm 16$ , and  $40 \pm 48$  kpc, respectively) that are consistent with zero. Similarly, GRB 061210 with extended emission has an offset of  $11 \pm 10$  kpc. An examination of the sample of Troja et al. (2008) reveals that their claim that short GRBs without extended emission have systematically larger offsets rests on four events in particular: GRBs 050509b, 060502b, 061217, and 061201. As noted above, GRBs 050509b and 061201 indeed appear to have substantial offsets<sup>16</sup>, but so do GRBs 071227 and 080503 with extended emission and offsets of about  $15$ – $20$  kpc. Next, the large offset for GRB 060502b relies on its claimed association with an elliptical galaxy  $70 \pm 16$  kpc from the XRT position (Bloom et al. 2007). However, the XRT error circle contains additional galaxies with negligible offsets (Berger et al. 2007). Finally, we note that the offset for GRB 061217 is unreliable due to a substantial discrepancy of about  $33^{+0}$  in the XRT positions from Butler (2007) and Evans et al. (2009). A continued investigation of the difference between short GRBs with and without extended emission will greatly benefit from the use of host-normalized offsets.

### 6.3. Light Distribution

In addition to projected offsets relative to the host center, we find that the locations of the short GRBs with *HST* imaging and sub-arcsecond positions are more diffusely distributed relative to their host light than long GRBs. In particular, we find that short GRB positions under-represent their host light, even in comparison to core-collapse and Type Ia SNe. This result is likely an upper limit on the brightness of short GRB locations since only the subset of events with optical afterglow positions can be studied with this approach. Thus, short GRBs arise from a population of events with a more diffuse distribution than massive stars and Type Ia SN progenitors. This result also indicates that the bulk of the progenitors of long and short GRBs cannot both be magnetars.

<sup>16</sup> We note that Troja et al. (2008) assume that the host of GRB 061201 is the galaxy at  $z = 0.111$  at an offset of about 32 kpc. However, as we have shown here based on the *HST* observations (Appendix B), there is a fainter potential host at a smaller offset.

There are currently 10 known short GRBs with optical afterglows for which *HST* observations will enable a similar analysis. This is twice the number of the current sample, and we can therefore make significant progress in understanding the relation of short GRB environments to the overall distribution of light in their host galaxies with future observations.

## 7. CONCLUSIONS

We presented the first comprehensive analysis of short GRB *HST* observations, and used these data to extract the morphological properties of the host galaxies, the projected physical and host-normalized GRB offsets, and the brightness at the location of the bursts relative to the overall light distribution of their hosts. The main conclusions of our analysis are as follows:

The majority of short GRB hosts are consistent with or have exponential surface brightness profiles, typical of late-type galaxies. This conclusion is in good agreement with results from spectroscopic observations that reveal star formation activity in  $\sim 3-4$  of short GRB hosts (Berger 2009).

The host galaxies of short GRBs are on average larger by about a factor of 2 than the hosts of long GRBs.

The observed short GRB offset distribution extends from  $\sim 1$  to 50 kpc, with a median of about 5 kpc. Including the short GRBs with only  $\gamma$ -ray or X-ray positions, we find that  $\sim 25\%$  of all events have offsets of  $\leq 10$  kpc, and  $\sim 5\%$  have offsets of  $\leq 20$  kpc. A additional, though softer, limit is that  $\sim 50\%$  have offsets of  $\leq 30$  kpc.

The observed physical offset distribution and the robust constraints compare favorably with the predicted distribution for NS-NS binaries. However, they do not rule out at least a partial contribution from other progenitor systems such as WD-WD binaries.

We find no convincing evidence that short GRBs with extended emission have smaller physical offsets than those without extended emission. In both sub-samples we find examples of both small offsets ( $\sim$  few kpc) and possibly large offsets (tens of kpc).

The distribution of host-normalized offsets for the subset of short GRBs with *HST* observations is nearly identical to that of long GRBs. This is due to the systematically larger size of short GRB hosts, and indicates that a comparison with long GRBs and progenitor models will benefit from the use of host-normalized (rather than physical) offsets.

The locations of short GRBs with sub-arcsecond positions and *HST* imaging under-represent the overall light distribution of their hosts, but less so in the red. This result differs substantially from long GRBs, core-collapse SNe, and even Type Ia SNe.

The results derived in this paper are based mainly on a small sample of short GRBs (9 events) from 2005-2006. Seven of these objects have precise positions based on optical afterglow detections. Ten additional events with precise afterglow positions, and a similar number with XRT positions (some of which with identified hosts), are now available for a similar study. It is essential to observe this existing sample, as well as new events from *Swift* and *Fermi*, with the refurbished *HST* using the ACS and WFPC3 instruments. In conjunction with constraints on the progenitor population from the redshift distribution (Berger et al. 2007) and spectroscopic studies of the host galaxies (Berger 2009), the continued use of high angular resolution imaging will provide crucial insight into the nature of the progenitors and the potential for multiple populations.

## APPENDIX

### THE HOST GALAXY OF GRB 060313

We present the first host galaxy association for GRB 060313, using *HST*/ACS observations in the F475W and F775W filters. The offset between the GRB position (determined from Gemini-South observations; Berger et al. 2007) and the galaxy center is about  $0.32''$  (Table 3). The galaxy brightness is  $m(\text{F475W}) = 26.4$  AB mag and  $m(\text{F775W}) = 25.6$  AB mag (Table 1). The probability of chance coincidence at this offset and galaxy brightness is only about  $3 \times 10^{-3}$  (Beckwith et al. 2006). We thus conclude that this galaxy is the likely host of GRB 060313.

### POSSIBLE HOST GALAXIES OF GRB 061201

The *HST* observations of GRB 061201 and its environment are shown in Figure 10. We explore two possibilities for the host galaxy. First, the burst is located  $16.2''$  (32.5 kpc) from a relatively bright galaxy at  $z = 0.111$  (marked ‘‘A’’ in Figure 10; Berger 2006; Stratta et al. 2007), for which we measure  $m(\text{F606W}) = 18.17$  and  $m(\text{F814W}) = 17.82$  AB mag. Second, we identify from the *HST*/ACS observations a second, fainter galaxy (marked ‘‘B’’ in Figure 10) located  $1.8''$  from the GRB position, and with  $m(\text{F606W}) = 25.34$  and  $m(\text{F814W}) = 25.03$  AB mag. The redshift of this galaxy is not known, but assuming  $z \sim 1$  the inferred projected offset is 14.2 kpc. The probability of chance coincidence for both galaxies is about 20% (Beckwith et al. 2006). We therefore do not claim a unique host galaxy association for this burst, and stress that both galaxies should be considered as potential hosts. Deeper *HST* observations may also uncover an underlying host.

### POSSIBLE HOST GALAXIES OF GRB 060502B

The *HST* observations of GRB 060502b and its environment are shown in Figure 8. Previously, Bloom et al. (2007) claimed that the host is likely an early type galaxy at  $z = 0.287$  located about 70 kpc away from the burst XRT position. These authors also note the presence of fainter objects within the XRT error circle. A galaxy with  $R = 25.2$  mag was also found by Berger et al. (2007). In the combined *HST*/ACS/F814W we find 6 faint galaxies within the XRT error circles of GRB 060502b (Figure 8). These galaxies have the following AB magnitudes: 27.5 (B), 25.9 (C), 27.2 (D), 26.1 (E), 24.8 (F), 25.7 (G). The probability of



chance coincidence for these galaxies within the XRT error circles is of the order of unity.

## REFERENCES

- Barbier, L., et al. 2007, GRB Coordinates Network, 6623, 1
- Barnes, J. E., & Hernquist, L. 1992, ARA&A, 30, 705
- Beckwith, S. V. W., et al. 2006, AJ, 132, 1729
- Belczynski, K., Perna, R., Bulik, T., Kalogera, V., Ivanova, N., & Lamb, D. Q. 2006, ApJ, 648, 1110
- Berger, E. 2006, GRB Coordinates Network, 5952, 1
- Berger, E. 2009, ApJ, 690, 231
- Berger, E., Cenko, S. B., Fox, D. B., & Cucchiara, A. 2009, ArXiv e-prints
- Berger, E., et al. 2007, ApJ, 664, 1000
- Berger, E., et al. 2005, Nature, 438, 988
- Bloom, J. S., Djorgovski, S. G., Kulkarni, S. R., & Frail, D. A. 1998, ApJ, 507, L25
- Bloom, J. S., Kulkarni, S. R., & Djorgovski, S. G. 2002, AJ, 123, 1111
- Bloom, J. S., et al. 2007, ApJ, 654, 878
- Bloom, J. S., & Prochaska, J. X. 2006, in American Institute of Physics Conference Series, Vol. 836, Gamma-Ray Bursts in the Swift Era, ed. S. S. Holt, N. Gehrels, & J. A. Nousek, 473
- Bloom, J. S., et al. 2006, ApJ, 638, 354
- Bloom, J. S., Sigurdsson, S., & Pols, O. R. 1999, MNRAS, 305, 763
- Butler, N. R. 2007, AJ, 133, 1027
- Ciotti, L., & Bertin, G. 1999, A&A, 352, 447
- Conselice, C. J., et al. 2005, ApJ, 633, 29
- D'Avanzo, P., et al. 2009, A&A, 498, 711
- Djorgovski, S. G., Kulkarni, S. R., Bloom, J. S., Goodrich, R., Frail, D. A., Piro, L., & Palazzi, E. 1998, ApJ, 508, L17
- Donaghy, T. Q., et al. 2006, ArXiv Astrophysics e-prints
- Eichler, D., Livio, M., Piran, T., & Schramm, D. N. 1989, Nature, 340, 126
- Evans, P. A., et al. 2009, MNRAS, 397, 1177
- Fox, D. B., et al. 2005, Nature, 437, 845
- Freeman, K. C. 1970, ApJ, 160, 811
- Fruchter, A. S., & Hook, R. N. 2002, PASP, 114, 144
- Fruchter, A. S., et al. 2006, Nature, 441, 463
- Fruchter, A. S., et al. 1999, ApJ, 519, L13
- Fryer, C. L., Woosley, S. E., & Hartmann, D. H. 1999, ApJ, 526, 152
- Gal-Yam, A., et al. 2006, Nature, 444, 1053
- Gehrels, N., et al. 2005, Nature, 437, 851
- Graham, J. F., et al. 2009, ApJ, 698, 1620
- Hjorth, J., et al. 2005, Nature, 437, 859
- Kelly, P. L., Kirshner, R. P., & Pahre, M. 2008, ApJ, 687, 1201
- Koekemoer, A. M., Fruchter, A. S., Hook, R. N., & Hack, W. 2002, in The 2002 HST Calibration Workshop : Hubble after the Installation of the ACS and the NICMOS Cooling System, ed. S. Arribas, A. Koekemoer, & B. Whitmore, 337
- Levan, A. J., et al. 2006a, ApJ, 648, L9
- Levan, A. J., Wynn, G. A., Chapman, R., Davies, M. B., King, A. R., Priddey, R. S., & Tanvir, N. R. 2006b, MNRAS, 368, L1
- Malesani, D., et al. 2007, A&A, 473, 77
- Metzger, B. D., Quataert, E., & Thompson, T. A. 2008, MNRAS, 385, 1455
- Narayan, R., Paczynski, B., & Piran, T. 1992, ApJ, 395, L83
- Ofek, E. O., et al. 2007, ApJ, 662, 1129
- Peng, C. Y., Ho, L. C., Impey, C. D., & Rix, H. W. 2007, in Bulletin of the American Astronomical Society, Vol. 38, Bulletin of the American Astronomical Society, 804
- Perley, D. A., Bloom, J. S., Modjaz, M., Miller, A. A., Shiode, J., Brewer, J., Starr, D., & Kennedy, R. 2008, GRB Coordinates Network, 7889, 1
- Perley, D. A., et al. 2009, ApJ, 696, 1871
- Piranomonte, S., et al. 2008, A&A, 491, 183
- Rau, A., McBreen, S., & Kruehler, T. 2009, GRB Coordinates Network, 9353, 1
- Sakamoto, T., Norris, J., Ukwatta, T., Barthelmy, S. D., Gehrels, N., & Stamatikos, M. 2007, GRB Coordinates Network, 7156, 1
- Schlegel, D. J., Finkbeiner, D. P., & Davis, M. 1998, ApJ, 500, 525
- Soderberg, A. M., et al. 2006, ApJ, 650, 261
- Stratta, G., et al. 2007, A&A, 474, 827
- Troja, E., King, A. R., O'Brien, P. T., Lyons, N., & Cusumano, G. 2008, MNRAS, 385, L10
- Trujillo, I., Erwin, P., Asensio Ramos, A., & Graham, A. W. 2004, AJ, 127, 1917
- Ukwatta, T. N., et al. 2009, GRB Coordinates Network, 9337, 1
- van den Bergh, S., Li, W., & Filippenko, A. V. 2005, PASP, 117, 773
- Wainwright, C., Berger, E., & Penprase, B. E. 2007, ApJ, 657, 367

TABLE 1  
*HST* OBSERVATIONS OF SHORT GRB HOST GALAXIES

GRB	RA (J2000)	Dec (J2000)	Uncert. ( <sup>00</sup> )	OA?	$z$	Instrument	Filter	Date (UT)	Exp. Time (s)	AB mag <sup>a</sup>	$A$ <sup>b</sup> (mag)
050509b	12 <sup>h</sup> 36 <sup>m</sup> 14.06 <sup>s</sup> 12 <sup>h</sup> 36 <sup>m</sup> 13.76 <sup>s</sup>	+28 59 <sup>00</sup> 7 2 <sup>00</sup> <sup>c</sup> +28 59 <sup>00</sup> 3 2 <sup>00</sup>	3.4 3.3	N	0.226	ACS	F814W	2005 May 14	6870	16.32	0.037
050709	23 <sup>h</sup> 01 <sup>m</sup> 26.96 <sup>s</sup>	-38 58 <sup>00</sup> 39 5 <sup>00</sup>	0.2	Y	0.1606	ACS WFPC2	F814W F450W	2006 Jul 16 2007 Jul 29	6981 3200	21.09 21.43	0.02 0.045
050724	16 <sup>h</sup> 24 <sup>m</sup> 44.38 <sup>s</sup>	-27 32 <sup>00</sup> 27 5 <sup>00</sup>	0.1	Y	0.257	WFPC2 WFPC2	F450W F814W	2008 Apr 07 2008 May 18	3200 3200	19.98 18.74	2.645 1.189
051210	22 <sup>h</sup> 00 <sup>m</sup> 41.26 <sup>s</sup> 22 <sup>h</sup> 00 <sup>m</sup> 41.33 <sup>s</sup>	-57 36 <sup>00</sup> 46 5 <sup>00</sup> -57 36 <sup>00</sup> 49 4 <sup>00</sup>	2.9 1.7	N	> 14	WFPC2	F675W	2007 Apr 03	2800	21.14	0.052
051221a	21 <sup>h</sup> 54 <sup>m</sup> 48.63 <sup>s</sup>	+16 53 <sup>00</sup> 27 4 <sup>00</sup>	0.2	Y	0.5465	WFPC2 WFPC2	F555W F814W	2007 Aug 13 2007 Aug 22	3200 1600	21.86 21.42	0.227 0.133
060121	09 <sup>h</sup> 09 <sup>m</sup> 51.99 <sup>s</sup>	+45 39 <sup>00</sup> 45 6 <sup>00</sup>	0.1	Y		ACS	F606W	2006 Feb 27	4400	26.22	0.0
060313	04 <sup>h</sup> 26 <sup>m</sup> 28.42 <sup>s</sup>	-10 50 <sup>00</sup> 39 9 <sup>00</sup>	0.2	Y		ACS ACS	F475W F775W	2006 Oct 13 2006 Oct 14	2088 2120	26.38 25.61	0.3 0.135
060502b	18 <sup>h</sup> 35 <sup>m</sup> 45.53 <sup>s</sup> 18 <sup>h</sup> 35 <sup>m</sup> 45.28 <sup>s</sup>	+52 37 <sup>00</sup> 52 9 <sup>00</sup> +52 37 <sup>00</sup> 54 7 <sup>00</sup>	3.7 5.8	N		ACS	F814W	2006 May 15-Jul 16	25224	17.88 / 24.8-27.5	0.085
061006	07 <sup>h</sup> 24 <sup>m</sup> 07.78 <sup>s</sup>	-79 11 <sup>00</sup> 55 5 <sup>00</sup>	0.2	Y	0.4377	ACS WFPC2	F814W F555W	2006 Oct 14 2008 May 22	6054 3200	21.67 23.90	0.616 1.052
061201	22 <sup>h</sup> 08 <sup>m</sup> 32.09 <sup>s</sup>	-74 34 <sup>00</sup> 47 1 <sup>00</sup>	0.2	Y	0.111 / <sup>e</sup>	ACS ACS	F606W F814W	2006 Dec 11 2006 Dec 11	2178 2244	18.17 / 25.34 <sup>f</sup> 17.82 / 25.03 <sup>f</sup>	0.251 0.147

NOTE. — Summary of short GRB positions and redshifts, *HST* observations, and host galaxy magnitudes (calculated using IRAF/ellipse).

<sup>a</sup> These values have been corrected for Galactic extinction.

<sup>b</sup> Galactic extinction.

<sup>c</sup> In all cases with *Swift*/XRT positions the top and bottom set of coordinates are from the catalogs of Butler (2007) and Evans et al. (2009), respectively.

<sup>d</sup> These magnitudes correspond to galaxy “A” and galaxies “B”–“G” in Figure 8.

<sup>e</sup> We consider two possible host galaxies for this burst (see Appendix B).

<sup>f</sup> The first value is for galaxy “A” and the second is for galaxy “B” in Figure 10.

TABLE 2  
MORPHOLOGICAL PROPERTIES OF SHORT GRB HOST GALAXIES

GRB	Instrument	Filter	galfit					IRAF/ellipse			
			$n^a$	$r_e$ ( <sup>0</sup> )	$r_e^c$ (kpc)	$e^b$ (AB mag arcsec <sup>-2</sup> )	AB Mag <sup>b</sup>	$n$	$r_e$ ( <sup>0</sup> )	$r_e^c$ (kpc)	$e^b$ (AB mag arcsec <sup>-2</sup> )
050509b	ACS	F814W	5.6	5.84	20.98	23.5	16.2	5.6	5.84	20.98	23.4
050709	ACS	F814W	1.1	0.76	2.08	23.0	21.2	0.6	0.64	1.75	22.4
	WFPC2	F450W	1.1	0.71	1.94	23.5	21.9	0.9	0.71	1.94	23.4
050724	WFPC2	F450W	4	1.35	5.34	23.2	19.4	1.3	0.36	1.42	20.8
	WFPC2	F814W	3.0	0.82	3.24	20.5	18.0	2.9	1.01	4.00	20.8
051210	WFPC2	F675W	1	0.70	5.63	23.8	23.7	1.0	0.63	5.07	24.2
			4	2.38	19.14	26.3	22.8				
051221a	WFPC2	F555W	0.9	0.36	2.29	23.3	23.1	0.8	0.34	2.17	23.1
	WFPC2	F814W	0.9	0.41	2.61	22.7	22.1	0.9	0.39	2.49	22.7
060121	ACS	F606W	1	0.36	2.89	25.9	27.1	1.4	0.67	5.39	27.2
			4	1.22	9.81	27.4	26.6				
060313	ACS	F475W	1	0.14	1.13	23.7	27.3	0.6	0.17	1.37	24.9
			4	0.32	2.57	26.2	26.7				
	ACS	F775W	1	0.07	0.56	21.4	26.1	1.3	0.23	1.85	25.0
			4	0.10	0.80	23.6	26.3				
061006	ACS	F814W	0.7	0.57	3.22	22.3	22.7	0.7	0.65	3.67	22.9
	WFPC2	F555W	1	0.63	3.55	23.3	23.4	0.8	0.55	3.10	23.6

NOTE. — Results of morphological analysis performed with `galfit` and `IRAF/ellipse` (§3).

<sup>a</sup> For the Sérsic index  $n$  in `galfit`, exact values of 1 and 4 indicate a fit with  $n$  as a fixed parameter.

<sup>b</sup> These values have been corrected for Galactic extinction.

<sup>c</sup> For the hosts with unknown redshift (GRBs 051210, 060121, and 060313) we assume  $z = 1$ .

TABLE 3  
SHORT GRB ANGULAR, PHYSICAL, AND HOST-NORMALIZED OFFSETS

GRB	Instrument	Filter	$z$	Reference	No.	GB: HST (mas)	$r_{\text{GRB}}$ (mas)	$r_{\text{gal}}$ (mas)	RA ( $^{\circ}$ )	Dec ( $^{\circ}$ )	Offset ( $^{\circ}$ )	Offset (kpc)	Offset ( $r_e^a$ )
050509b	ACS	F814W	0.226	SDSS	10	30	3400 3300	1.0 1.0	+15.61 +11.68	+8.40 +4.40	17.73 3.4 12.48 3.3	63.7 12.2 44.8 11.9	3.04 0.58 2.14 0.57
050709	ACS WFPC2 ACS	F814W F450W F814W	0.1606	HST/ACS HST/ACS self	35 12	8 14	1.0 1.0	1.4 <sup>b</sup> 4.7 1.0	+1.294 +1.306 1.4	-0.310 -0.360 +1.329	1.331 0.010 1.355 0.020 -0.310 1.365	3.64 0.027 3.71 0.055 0.002 3.74	2.08 0.02 1.91 0.03 0.005 2.13
050724	WFPC2 WFPC2 PANIC	F450W F814W $K_s$	0.257	Magellan/PANIC Magellan/PANIC self	60 85	15 14	5.0 5.0	4.7 <sup>c</sup> 1.4 5.0	-0.226 -0.213 1.0	-0.640 -0.630 -0.253	0.679 0.025 0.665 0.020 -0.650 0.697	2.69 0.099 2.63 0.079 0.006 2.76	1.89 0.07 0.66 0.02 0.024
051210	WFPC2	F675W	> 1.4	2MASS	12	29	2900 1700	8 8	+2.89 +3.45	+0.50 -2.40	2.93 2.9 4.20 1.7	24.9 24.6 35.7 14.4	4.65 4.60 6.67 2.70
051221	WFPC2 WFPC2	F555W F814W	0.5465	Gemini-N/GMOS Gemini-N/GMOS	45 45	23 24	2.5 2.5	3.1 3.1	-0.287 -0.330	+0.090 +0.090	0.301 0.029 0.342 0.030	1.92 0.18 2.18 0.19	0.88 0.08 0.88 0.08
060121	ACS	F606W		Gemini-N/GMOS	25	18	16	12	-0.115	+0.030	0.119 0.046	0.96 0.37	0.18 0.07
060313	ACS ACS	F475W F775W		Gemini-S/GMOS Gemini-S/GMOS	30 15	30 30	19 19	19.4 13.2	+0.354 +0.280	+0.040 +0.050	0.356 0.068 0.284 0.062	2.86 0.55 2.28 0.50 <sup>d</sup>	2.09 0.40 1.23 0.23
060502b	ACS	F814W		USNO-B	47	120	3700 5800	<sup>e</sup> <sup>e</sup>					
061006	ACS WFPC2	F814W F555W	0.4377	VLT/FORS1 VLT/FORS1	75 45	17 20	21 21	4.9 11	-0.155 -0.171	-0.170 -0.190	0.230 0.043 0.256 0.052	1.30 0.24 1.44 0.29	0.35 0.07 0.46 0.10
061201	ACS ACS	F814W F606W		VLT/FORS2 VLT/FORS2	24 24	13 13	41 41	<sup>e</sup> <sup>e</sup>					

NOTE. — Projected angular, physical, and host-normalized offsets for the short GRBs with *HST* observations.

<sup>a</sup> Values for  $r_e$  are from `ellipse` (Table 2).

<sup>b</sup> Systematic uncertainty in host center is 50 mas.

<sup>c</sup> Systematic uncertainty in host center is 20 mas.

<sup>d</sup> Assuming  $z = 1$ .

<sup>e</sup> We do not claim a unique host galaxy identification for this burst.

TABLE 4  
SHORT GRB FRACTIONAL FLUX

GRB	Instrument	Filter	Fractional Flux
050709	WFPC2	F450W	0
	ACS	F814W	0.09
050724	WFPC2	F450W	0.03
	WFPC2	F814W	0.33
051221	WFPC2	F555W	0.54
	WFPC2	F814W	0.65
060121	ACS	F606W	0.41
060313	ACS	F475W	0.04
	ACS	F775W	0
061006	WFPC2	F555W	0.56
	ACS	F814W	0.63

NOTE. — Fraction of host galaxy light in pixels fainter than the GRB position.

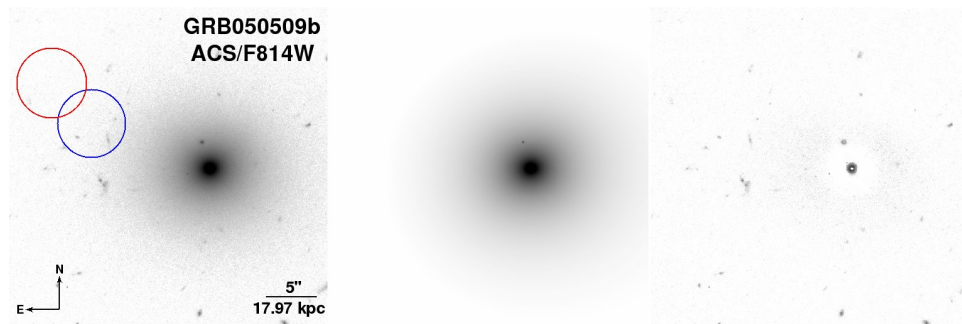


FIG. 1.— *Left*: *HST*/ACS/F814W image of the location of GRB 050509b. The circles mark the X-ray positions of the afterglow from the analysis of Butler (2007) (red) and Evans et al. (2009) (blue). *Center*: Sérsic model fit from `galfit`. *Right*: Residual image.

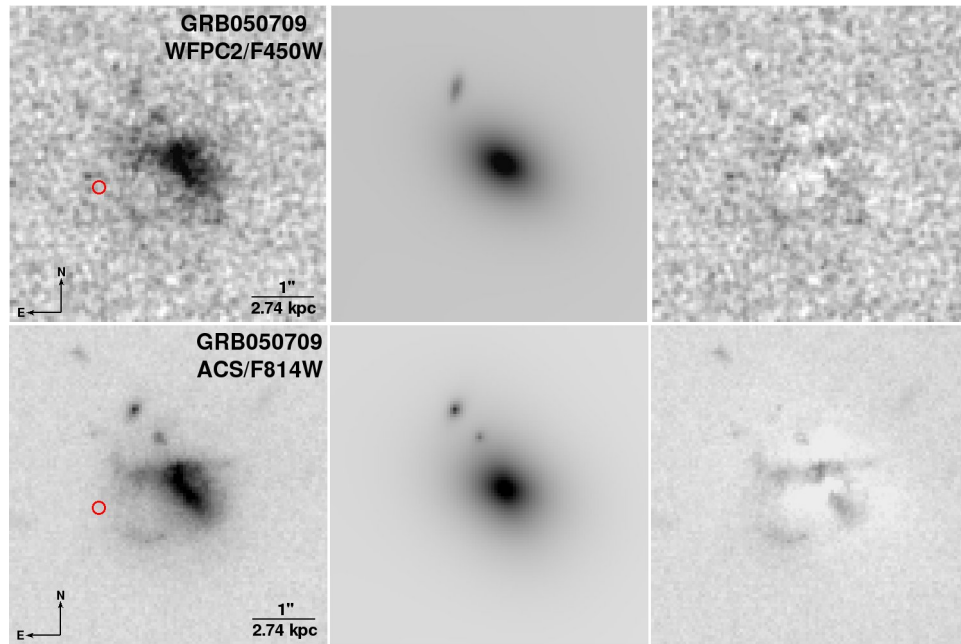


FIG. 2.— *Top-left*: *HST*/ACS/F450W image of the host galaxy of GRB 050709 with a  $10''$  error circle representing the afterglow position. *Top-center*: Sérsic model fit from `galfit`. *Top-right*: Residual image. *Bottom*: Same, but for the *HST*/WFPC2/F814W observations.

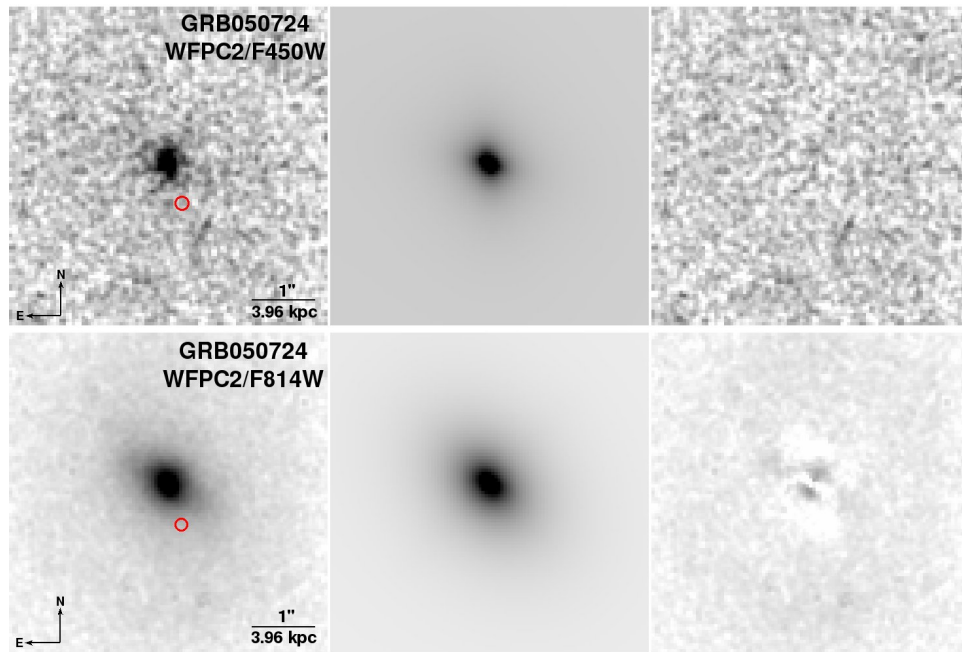


FIG. 3.— *Top-left*: *HST*/WFPC2/F450W image of the host galaxy of GRB 050724 with a 5'' error circle representing the afterglow position. *Top-center*: Sérsic model fit from `galfit`. *Top-right*: Residual image. *Bottom*: Same, but for the *HST*/WFPC2/F814W observations.



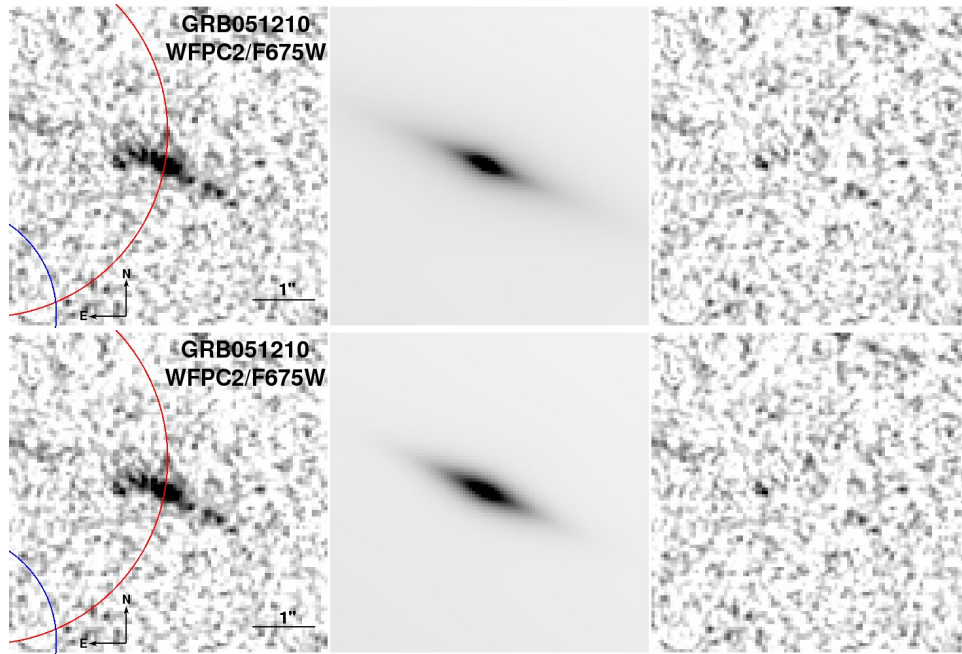


FIG. 4.— *Top-left*: *HST*/WFPC2/F675W image of the location of GRB 051210. The circles mark the X-ray positions of the afterglow from the analysis of Butler (2007) (red) and Evans et al. (2009) (blue). *Top-center*: Sérsic model fit from `galfit` with a fixed value of  $n = 1$ . *Top-right*: Residual image. *Bottom*: Same, but for Sérsic model fit from `galfit` with a fixed value of  $n = 4$ .

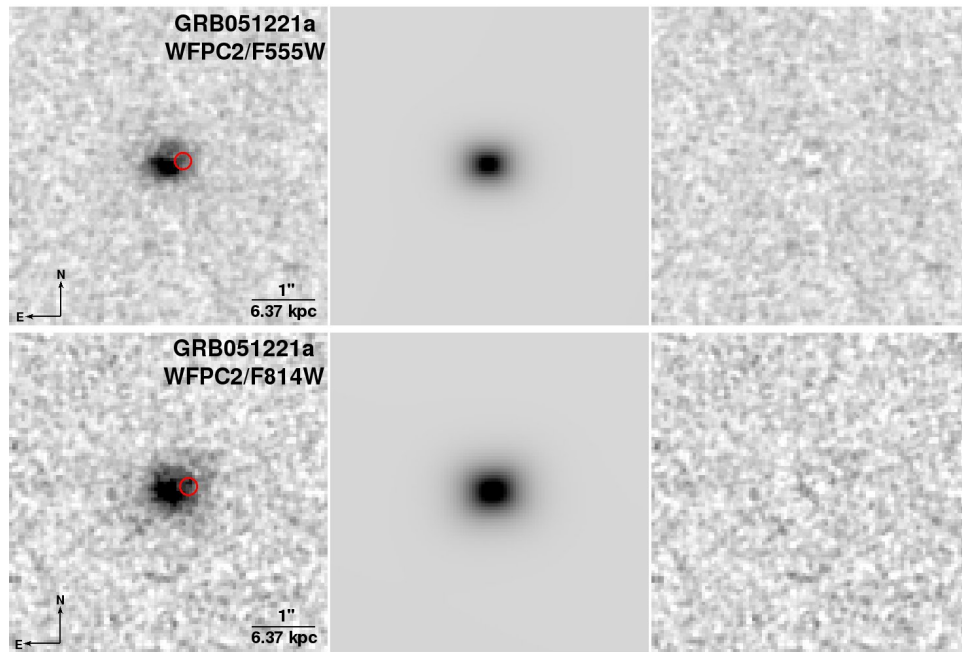


FIG. 5.— *Top-left*: *HST*/WFPC2/F555W image of the host galaxy of GRB 051221 with a  $5''$  error circle representing the afterglow position. *Top-center*: Sérsic model fit from `galfit`. *Top-right*: Residual image. *Bottom*: Same, but for the *HST*/WFPC2/F814W observations.

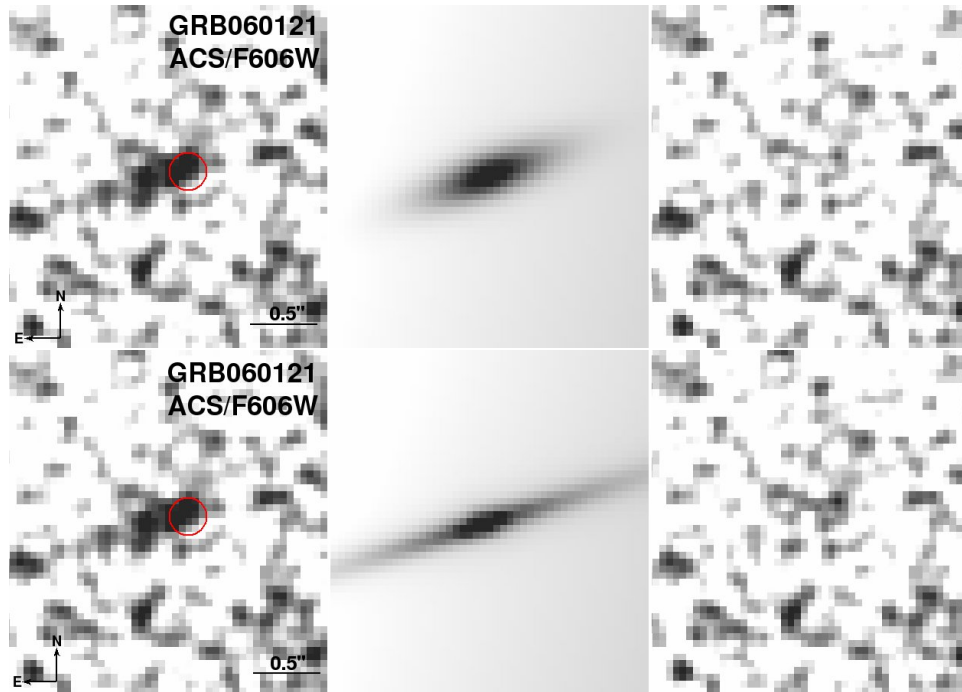


FIG. 6.— *Top-left*: *HST*/ACS/F606W image of the host galaxy of GRB 060121 with a 3'' error circle representing the afterglow position. The image has been smoothed with a 2 × 2 pixel Gaussian. *Top-center*: Sérsic model fit from `galfit` with a fixed value of  $n = 1$ . *Top-right*: Residual image. *Bottom*: Same, but for Sérsic model fit from `galfit` with a fixed value of  $n = 4$ .

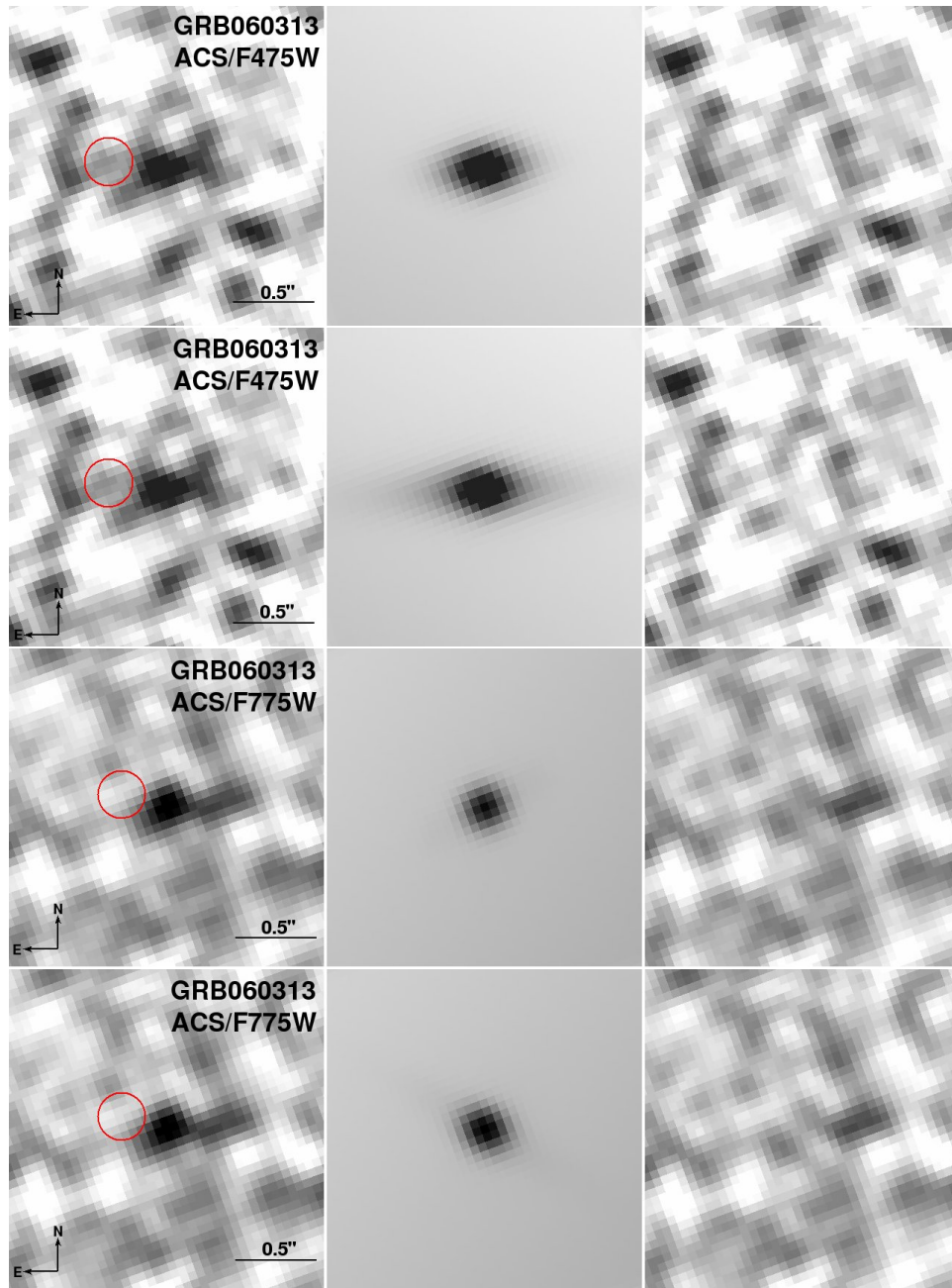


FIG. 7.— *Top-left*: *HST*/ACS/F475W image of the host galaxy of GRB 060313 with a  $3 \times 3$  error circle representing the afterglow position. The image has been smoothed with a  $3 \times 3$  pixel Gaussian. *Top-center*: Sérsic model fit from `galfit` with a fixed value of  $n = 1$ . *Top-right*: Residual image. *Second panel*: Same, but for Sérsic model fit from `galfit` with a fixed value of  $n = 4$ . *Third panel*: Same, but for the *HST*/WFPC2/F775W observations with a fixed value of  $n = 1$ . *Bottom panel*: Same, but for the *HST*/WFPC2/F775W observations with a fixed value of  $n = 4$ .

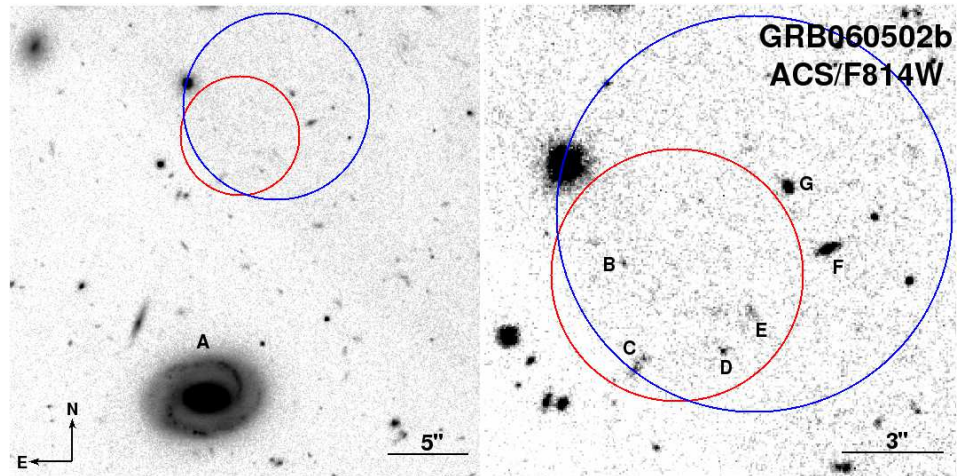


FIG. 8.— *HST*/ACS/F814W images of the host galaxy of GRB 060502b. The circles mark the X-ray positions of the afterglow from the analysis of Butler (2007) (red) and Evans et al. (2009) (blue). The bright galaxy marked “A” is located at  $z = 0.287$  (Bloom et al. 2007). Several fainter galaxies (“B”–“G”) are located within the XRT error circles (see Appendix C).

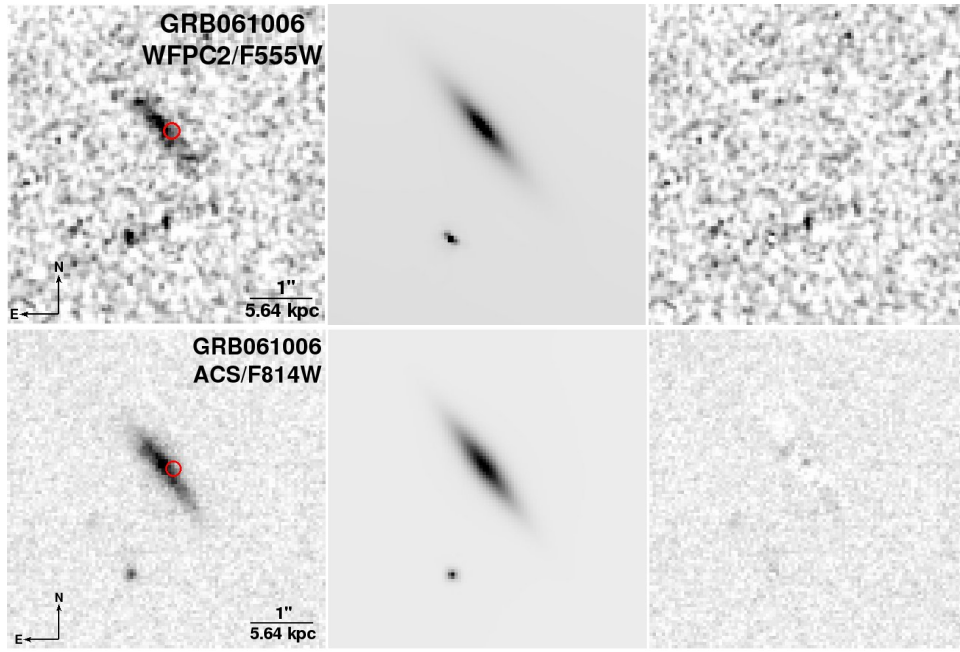


FIG. 9.— *Top-left*: *HST*/ACS/F555W image of the host galaxy of GRB 061006 with a 3 $\sigma$  error circle representing the afterglow position. *Top-center*: Sérsic model fit from *galfit*. *Top-right*: Residual image. *Bottom*: Same, but for the *HST*/ACS/F814W observations.

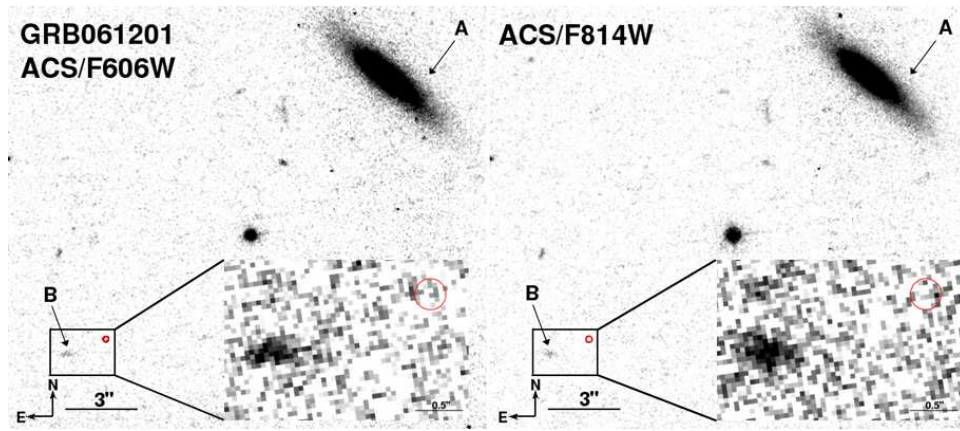


FIG. 10.— *Left*: *HST*/ACS/F606W image of the location of GRB 061201. The bright galaxy at the upper right-hand corner (“A”) is located at  $z = 0.11$  (Berger 2006; Stratta et al. 2007) with an offset of about 32.5 kpc. A second, fainter galaxy (“B”) is located about  $1 \text{ kpc}$  away from the optical afterglow position (see Appendix B). *Right*: Same, but for the *HST*/ACS/F814W observations.

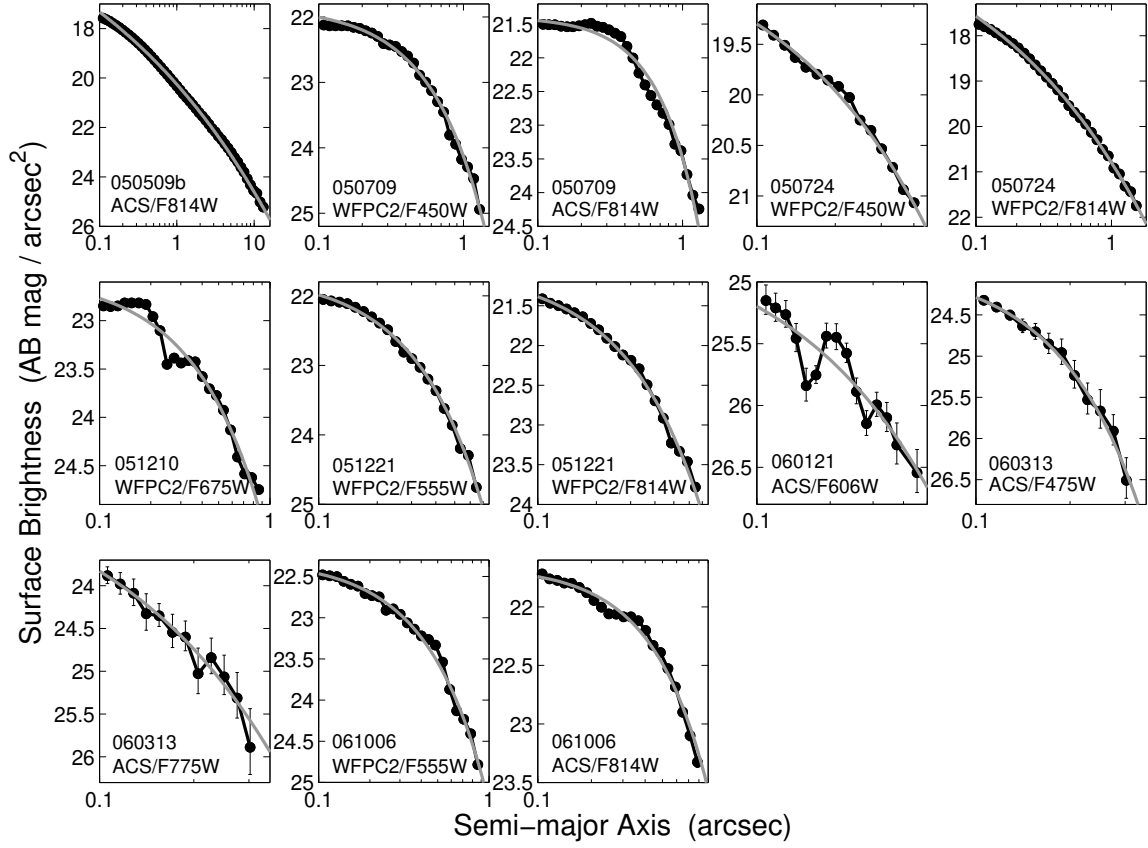


FIG. 11.— One-dimensional radial surface brightness profiles for short GRB host galaxies derived from IRAF/ellipse. The gray lines are Sérsic model fits (Equation 1) to the surface brightness profiles. The results of the fits are listed in Table 2.



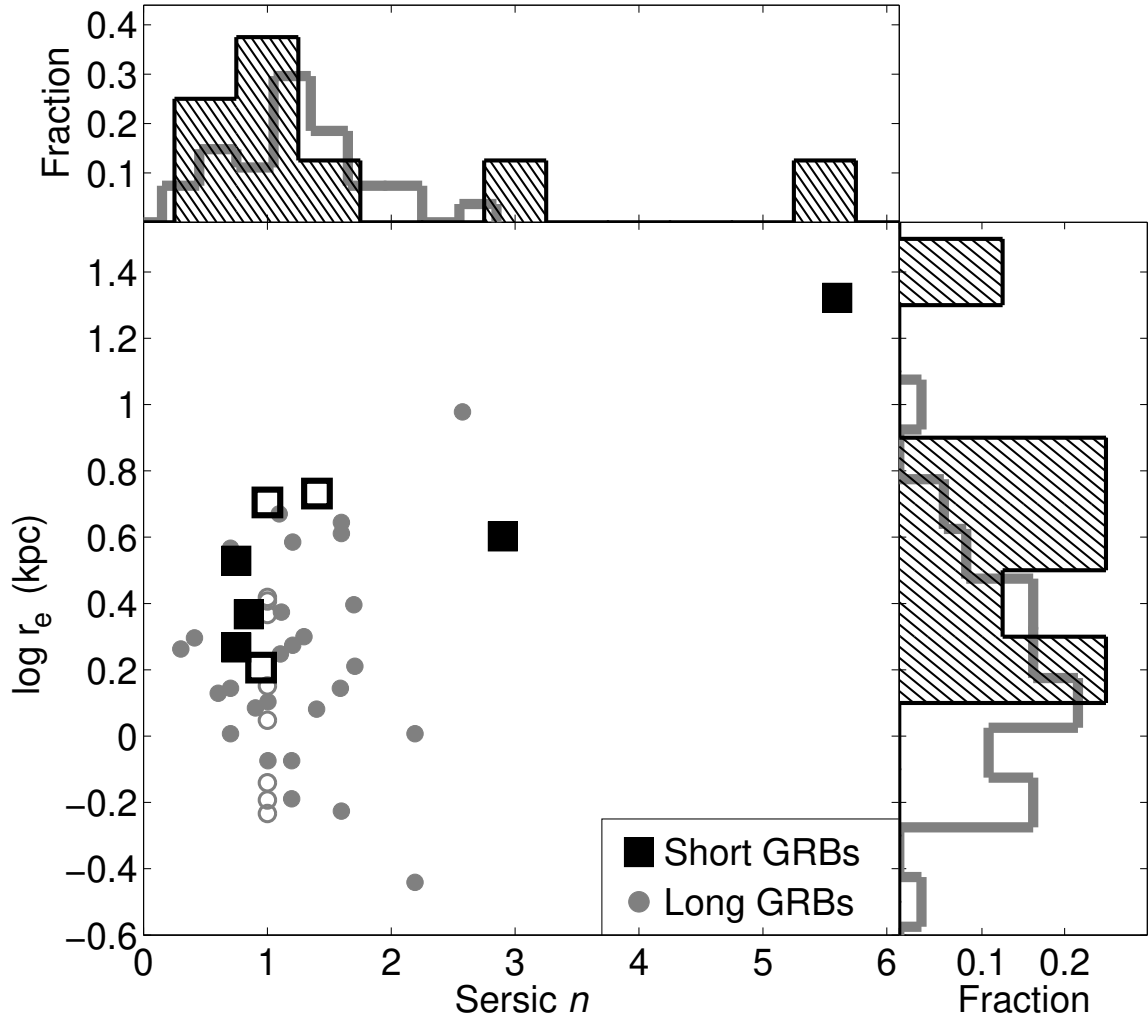


FIG. 12.— Effective radii for the short GRB hosts with *HST* observations plotted as a function of their Sérsic  $n$  values. We use the results of the IRAF/ellipse analysis; see Figure 11 (open squares designate hosts for which `galfit` models with  $n = 1$  and  $n = 4$  provide an equally good fit). Also shown are the data for long GRB hosts based on *HST* observations from the sample of Wainwright et al. (2007). The hosts of GRBs 050509b and 050724 have  $n$  values typical of elliptical galaxies, but the remaining hosts have a similar distribution to that of long GRBs (i.e., a median of  $n \approx 1$ , or an exponential disk profile). On the other hand, the hosts of short GRBs are larger by about a factor of 2 than the hosts of short GRBs, in agreement with their higher luminosities.

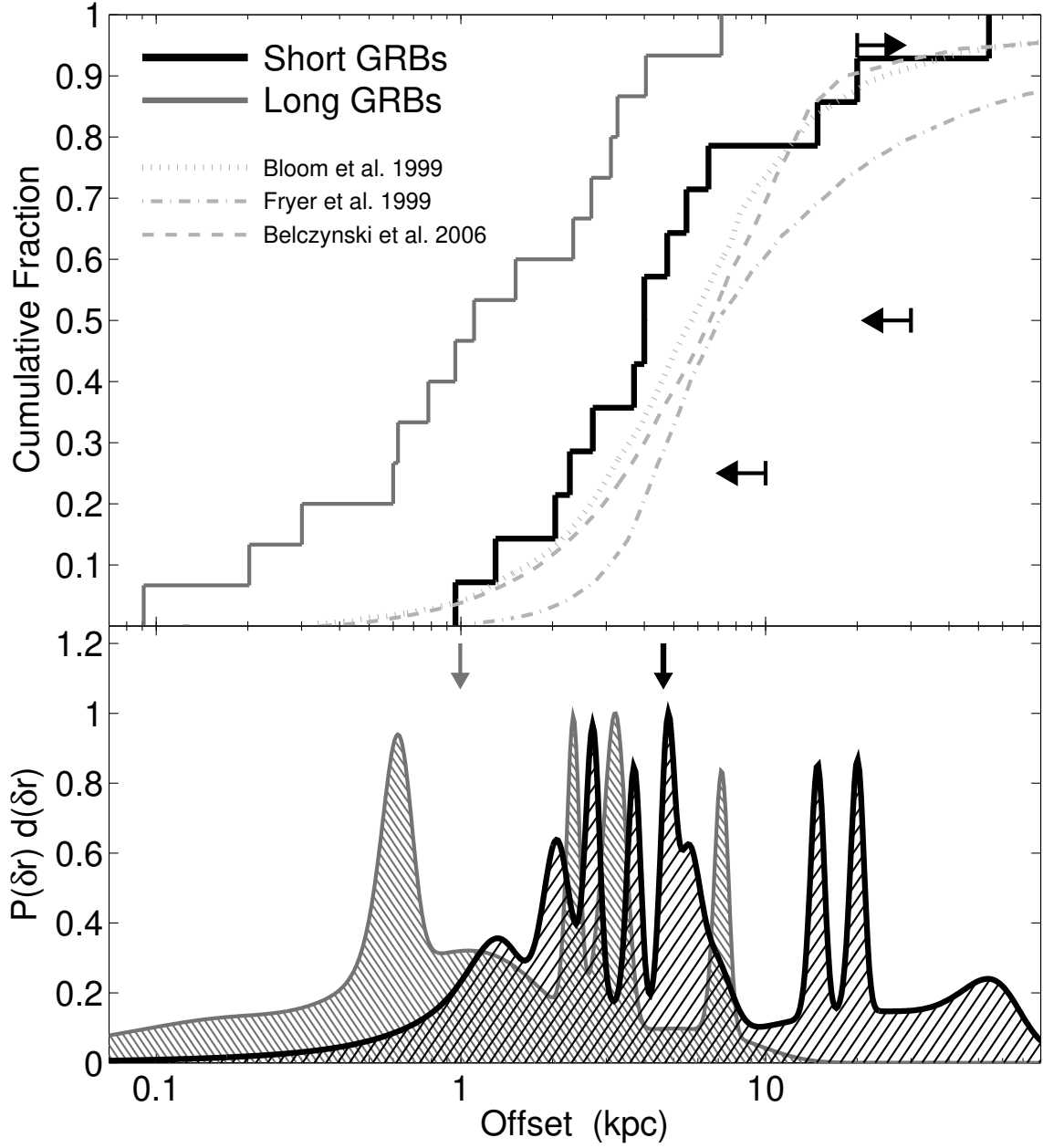


FIG. 13.— Projected physical offsets for short GRBs (black) and long GRBs (gray; Bloom et al. 2002). The top panel shows a cumulative distribution, while the bottom panel shows the differential distribution taking into account the non-Gaussian errors on the offsets. The arrows in the bottom panel mark the median value for each distribution. The median value for short GRBs,  $\sim 5$  kpc, is about a factor of 5 times larger than for long GRBs. The arrows in the top panel exhibit the most robust constraints on the offset distribution (§4), taking into account the fraction of short GRBs with only  $\gamma$ -ray positions, as well as short GRBs for which hosts have been identified within XRT error circles (thereby providing a typical range of  $\sim 0-30$  kpc). Also shown in the top panel are predicted offset distributions for NS-NS binary mergers in Milky Way type galaxies based on population synthesis models. We find good agreement between the observed distribution and models, as well as between the robust constraints and models.

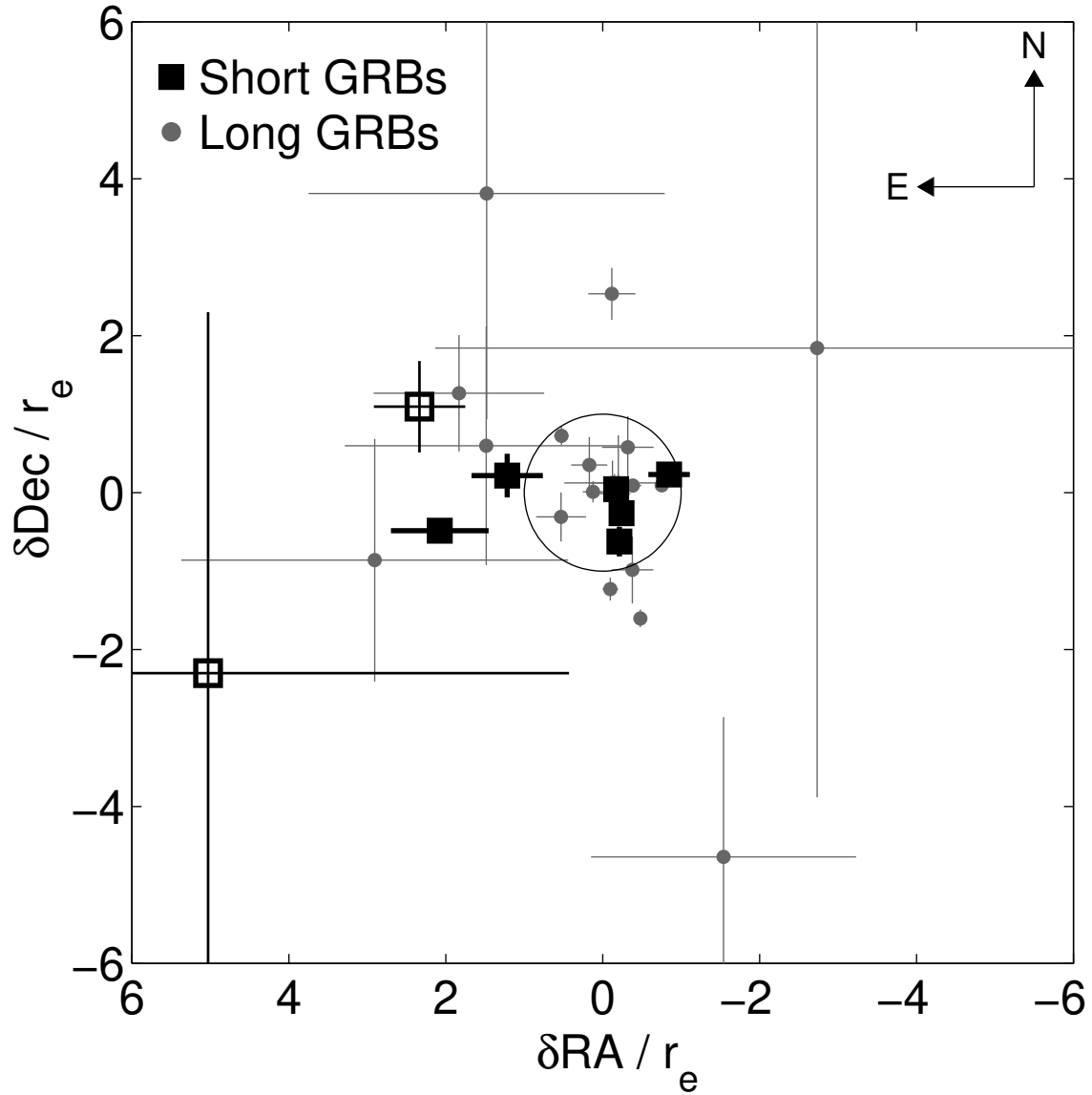


FIG. 14.— Host-normalized offsets in right ascension and declination for the short GRBs in our *HST* sample (black; open symbols mark the GRBs with X-ray positions, 050509b and 051210). Also shown are the offsets for long GRBs from the sample of Bloom et al. (2002). The circle marks an offset of  $1 r_e$ . About half of all long GRBs have offsets of  $\leq 1 r_e$ , and we find a similar result for short GRBs.

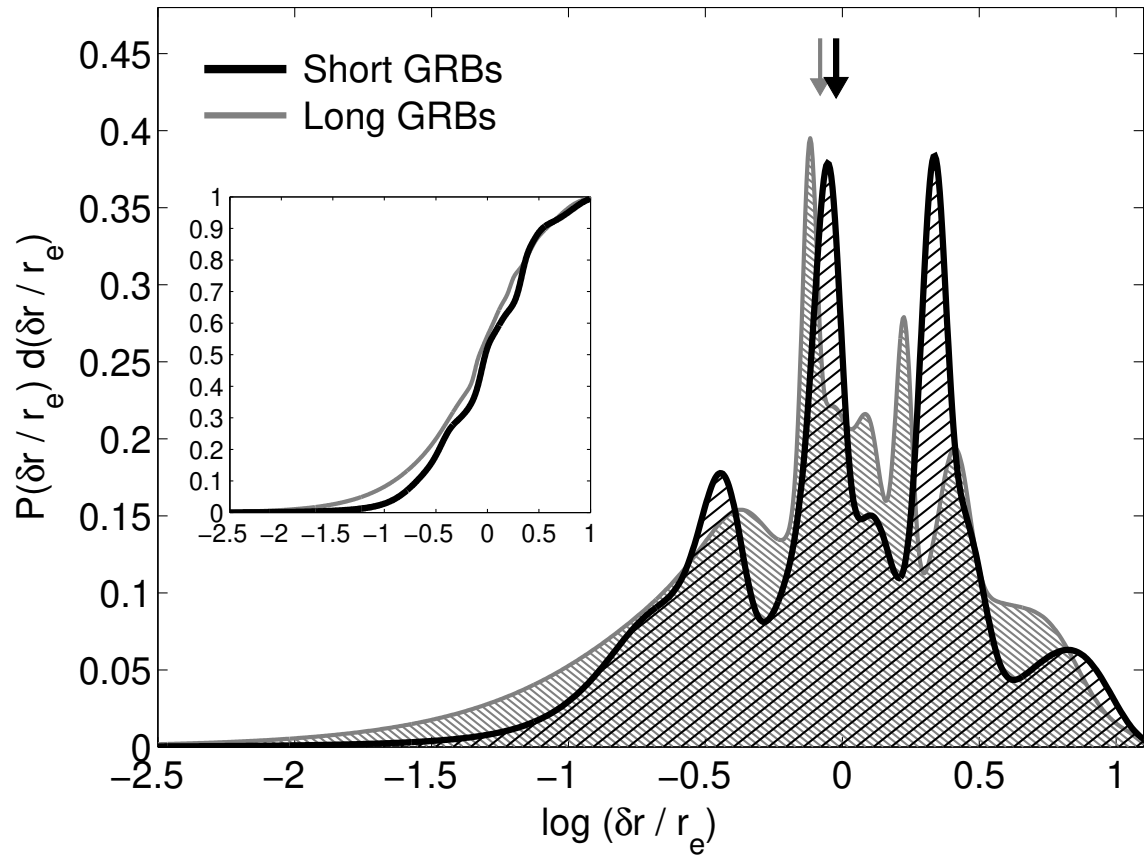


FIG. 15.— Probability distributions of the host-normalized offsets of short GRBs (black) and long GRBs (gray; Bloom et al. 2002). For each burst we include the host-normalized offset taking into account the non-Gaussian errors. The arrows mark the median value of each distribution, and the inset shows the cumulative distribution.

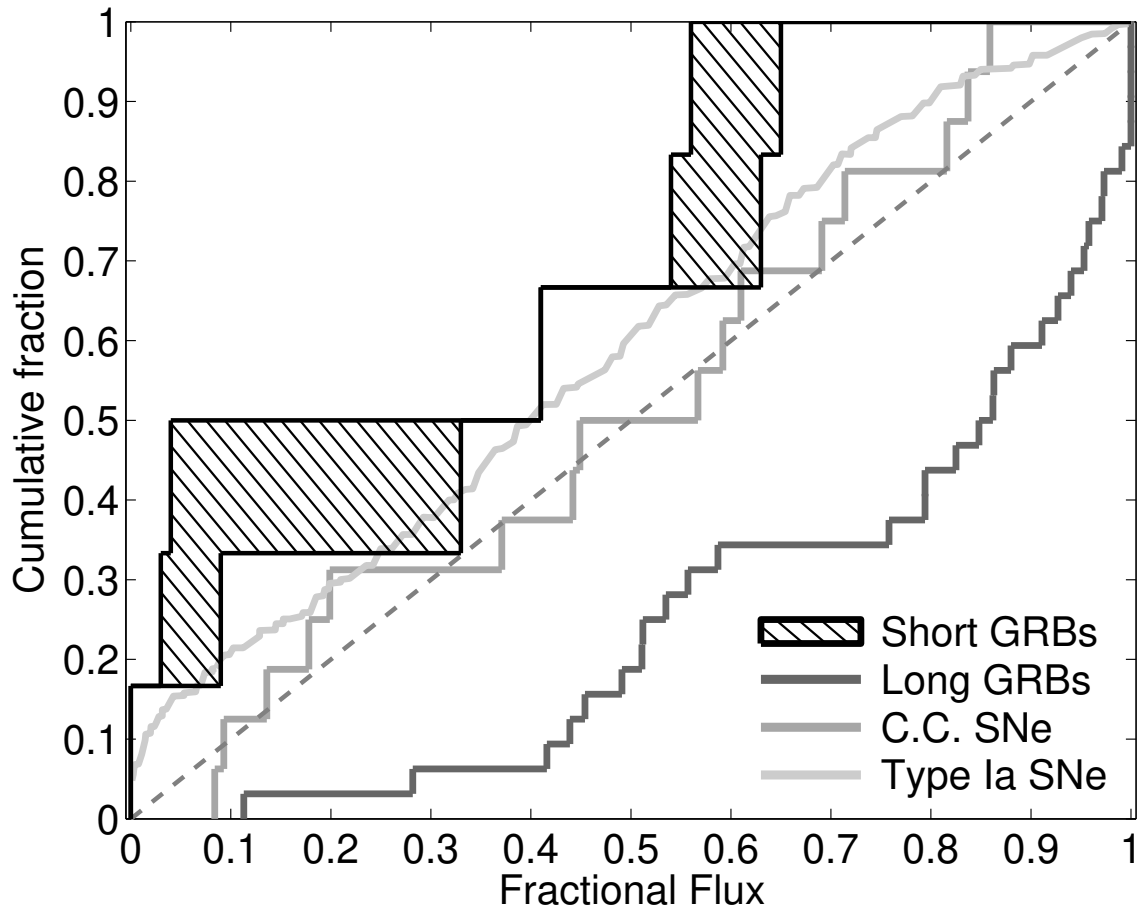


FIG. 16.— Cumulative distribution of fractional flux at the location of short GRBs relative to their host light. For each burst we measure the fraction of host light in pixels fainter than the GRB pixel location. The shaded area is defined by the results for the two available filters for each short GRB. Also shown are data for long GRBs (dark gray line) and for core-collapse and Type Ia SNe (light gray lines) from Fruchter et al. (2006) and Kelly et al. (2008). The dashed line marks the expected distribution for objects which track their host light distribution. Short GRBs appear to under-represent their host light, while long GRBs tend to be concentrated in the brightest regions of their hosts (Fruchter et al. 2006).